Disruption of WSB2-mediated NOXA Degradation Induces Synthetic Lethality to Anti-apoptotic BCL-2 Family Protein Inhibitors

Dongyue Jiao[1,8], Kun Chang[2,3,8], Yingji Chen[1], Jiamin Jin[1], Ren Mo[4], Yucong Zhang[5], Kun Gao[6,7], Yaoting Xu[8,*], Lixin Wang[5,*], and Chenji Wang[1,*]

[1]State Key Lab of Genetic Engineering, Shanghai Stomatological Hospital & School of Stomatology, MOE Engineering Research Center of Gene Technology, Shanghai Engineering Research Center of Industrial Microorganisms, School of Life Sciences, Fudan University, Shanghai 200438, P.R. China

[2]Department of Urology, Fudan University Shanghai Cancer Center, Shanghai, 200032, China;

[3]Department of Oncology, Shanghai Medical College, Fudan University, Shanghai 200032, China;

[4]Department of Urology, Inner Mongolia Urological Institute, Inner Mongolia Autonomous Region people's Hospital, Hohhot 010017, Inner Mongolia, China

[5]Department of Clinical Laboratory, Shanghai First Maternity and Infant Hospital, School of Medicine, Tongji University, Shanghai 200092, China

[6]Department of Vascular Surgery, Zhongshan Hospital, Fudan University, Shanghai, China.

[7]Shanghai Key Laboratory of Maternal and Fetal Medicine, Shanghai First Maternity and Infant Hospital, Shanghai 200092, China

[8]Department of Urology, Shanghai Fourth People's Hospital Affiliated to Tongji University School of Medicine, Shanghai 200434, China.

*Correspondence: chenjiwang@fudan.edu.cn (C.W); 2000019@tongji.edu.cn (Y.X).

Abstract

Anti-apoptotic BCL-2 family proteins are frequently overexpressed in various cancers, contributing to the initiation and development of cancer, as well as intrinsic or acquired resistance to therapy. Although BCL-2 family protein inhibitors, such as Venetoclax, have demonstrated efficacy in hematological neoplasms, their effectiveness as single agents in solid tumors is limited. Identifying alternative molecular targets that can overcome intrinsic resistance to BCL-2 family protein inhibitors is of great clinical importance. Here, we present evidence of strong synthetic lethal interactions between WSB2, a relatively unexplored substrate-binding receptor of the Cullin 5-RBX2-Elongin B/C (CRL5) E3 ubiquitin ligase complex, and multiple anti-apoptotic BCL-2 family proteins. Mechanistically, an assembled $CRL5^{WSB2}$ E3 ubiquitin ligase complex targets NOXA, a pro-apoptotic BCL-2 family protein, for degradation via the ubiquitin-proteasomal pathway. Ablation of WSB2 leads to a remarkable accumulation of NOXA proteins in cultured cell lines and knockout mouse organs. While WSB2 deficiency alone has a minimal effect on spontaneous apoptosis, it renders cancer cells more susceptible to apoptosis when anti-apoptotic BCL-2 family proteins are genetically depleted or pharmacologically inhibited. These findings establish WSB2 as a critical regulator of mitochondrial apoptosis and highlight the dysregulation of the WSB2-NOXA regulatory axis as a contributing factor to apoptosis resistance in cancer cells. Synergistically targeting WSB2 and anti-apoptotic BCL-2 family proteins holds promising clinical potential in the treatment of human cancers.

Keywords:

Apoptosis, BCL-2, WSB2, Cullin, Ubiquitination, Venetoclax

Introduction

One of the major hallmarks of human cancers is their inherent or developed resistance to apoptosis, a type of programmed cell death[1]. This evasive mechanism contributes significantly to both tumor initiation and progression, as well as the resistance observed in many cancer treatments. Importantly, most anticancer therapies available—including chemotherapy, radiotherapy, molecularly targeted therapy, and immunotherapy—work primarily by initiating cell death pathways like apoptosis in cancer cells[2].

Apoptosis is primarily regulated at the mitochondrial level by the B-cell lymphoma protein-2 (BCL-2) family of proteins. This family is bifurcated into two primary categories: anti-apoptotic proteins and pro-apoptotic proteins. Anti-apoptotic proteins, such as BCL-2, BCL-XL, BCL-W, and MCL-1, harbor between one to four BH domains and play essential roles in maintaining outer mitochondrial membrane integrity by inhibiting their pro-apoptotic counterparts. Pro-apoptotic proteins further segregate into multidomain effector proteins (e.g., BAK, BAX, and BOK) that contain multiple BH domains, and an array of "BH3-only" proteins, named for their single conserved BH3 domain (e.g., BIM, PUMA, NOXA, BAD, and BID). Various cell death stimuli can activate or induce these proapoptotic entities, driving mitochondrial outer membrane permeabilization followed by apoptosis. The anti-apoptotic members of the BCL-2 family have restrainer BH3-binding grooves that help to regulate the activity of "BH3-only" and multidomain effector proteins[3, 4]. Notably, tumors often acquire resistance to apoptosis through overexpression of anti-apoptotic proteins or downregulation/mutation of pro-apoptotic ones, underscoring the need for therapeutic strategies targeted at this critical cellular balance[5].

A unique class of small molecule BH3-mimetics has been developed, which specifically target and block the anti-apoptotic BCL-2 family proteins. Among these inhibitors, ABT-199 (Venetoclax) has been approved for clinical use against BCL-2 dependent tumors, especially in patients with small lymphocytic lymphoma (SLL) or chronic lymphocytic leukemia (CLL) who have undergone at least one prior therapy[5]. Furthermore, Venetoclax can be combined with

other drugs to treat acute myeloid leukemia (AML)[6, 7]. Despite major breakthroughs in hematological neoplasms, the effectiveness of these drugs in solid tumors is limited, possibly due to their reduced dependence on BCL-2 compared to hematological neoplasms[8]. Searching for new actionable targets to sensitize solid tumor cells to BCL-2 inhibitor-mediated cytotoxicity is a promising avenue for investigation.

Cullin 5 (CUL5), a member of the cullin-RING ubiquitin ligase family, is a core component of multisubunit E3 ubiquitin-protein ligase complexes which catalyze the conjugation of ubiquitin moieties onto specific protein substrates. CUL5 interacts with RBX2, Elongin B/C, and a SOCS Box-containing substrate-binding receptor to assembly a CRL5 E3 ubiquitin ligase protein complex[9]. WD Repeat and SOCS Box Containing 2 (WSB2), has been classified as a substate receptor for the CRL5 E3 ubiquitin ligase complex[10]. WSB2 has been shown to be overexpressed in several cancers (lung cancer, breast cancer, and melanoma) and promote malignant biological behavior, such as proliferation, cycle progression, and migration[11-13]. However, a lack of reported physiological substrates for the $CRL5^{WSB2}$ complex impedes recognizing WSB2 as a potentially targetable oncoprotein for therapeutic interventions.

By analyzing the gene co-dependency dataset deposited in the DepMap Portal (https://depmap.org/), we have unveiled a potential functional interplay between WSB2 and multiple BCL-2 family proteins. Biochemical analyses demonstrate that WSB2 acts as a substrate-binding receptor of CRL5 E3 to promote NOXA turnover. A series of functional analyses were performed in cell lines, xenograft tumor models, and knockout mice models to explore the biological significance and clinical relevance of WSB2-mediated regulation of mitochondrial apoptosis. These findings highlight the clinical potential of targeting WSB2 for synthetic lethality with BCL-2 family inhibitor treatment in human cancers.

Results

Multiple BCL-2 family proteins were identified as interactors of WSB2

To elucidate the unidentified molecular functions of WSB2, we analyzed the genetic co-dependency between WSB2 and other proteins using Broad's 21Q2 DepMap dataset[14]. This dataset, derived from large-scale loss-of-function sgRNA screens for vulnerabilities in 990

cancer cell lines, allows the identification of genes with similar functions or pathways[15, 16]. Gene ontology analysis of the top 100 co-dependent genes of WSB2 revealed a significant enrichment in multiple apoptosis-related processes (**Supplementary Figure 1A**, **Supplementary Table. 1, 2**). Among the top four correlated genes, WSB2 showed a positive correlation with anti-apoptotic BCL2L2 (BCL-W) and MCL-1, but a negative correlation with pro-apoptotic BAX and PMAIP1 (NOXA) (**Figure 1A**). Notably, WSB2, along with BCL-2, BCL-W, BAX, MCL-1, NOXA, and BAK1, formed a co-essential module[17] that also includes UBE2J2/MARCH5, an E2-E3 ligase complex responsible for MCL1/NOXA turnover (**Figure 1B**)[18-20]. Through utilizing a web server, DepLink[21], to identify genetic and pharmacological perturbations that produce similar impacts on cell viability, as determined by DepMap and drug sensitivity datasets obtained from two high-throughput pharmacological screenings[22, 23], we observed that WSB2 knockout exhibited the highest correlations with two BH3-mimetics (ABT-737, ABT-263), out of hundreds of drugs tested (**Supplementary Figure 1B, C, Supplementary Table 3**). These molecular links prompted us to investigate whether WSB2 has any impact on mitochondrial apoptosis through the regulation of BCL-2 family proteins. To test this hypothesis, we initially examined the potential interaction between WSB2 and BCL-2 family proteins. Exogenous co-IP assay results indicated that among the eight tested BCL-2 family proteins, WSB2 interacted with MCL-1, NOXA, BAD, BCL-W, and BCL-2, but not with BAX, BCL-W, and BAK (**Figure 1C**). These interactions were further confirmed by semi-endogenous or endogenous co-IP assays (**Figure 1D, F-J**). In comparison, WSB1, a closely related paralog of WSB2, did not interact with these BCL-2 family proteins (**Figure 1E**).

Considering that BCL-2 family proteins are located on the outer mitochondrial membrane, we investigated whether WSB2 was also located on the mitochondria. Immunofluorescent analysis revealed that WSB2 is localized throughout the cytoplasm, with a fraction of it colocalizing with the mitochondrial marker HSP60 (**Figure 1K**). We further separated the nuclear, mitochondrial, and cytoplasmic fractions of HeLa cells using density-gradient centrifugation methods. WSB2 predominantly localizes in the cytoplasm, with a moderate fraction in the mitochondria, while its presence in the nucleus is minor (**Figure. 1L**). To determine the submitochondrial localization of WSB2, we purified mitochondria from HeLa

cells and performed Protease K digestion experiments with different mitochondrial preparations. Cleavage by Protease K only occurred in intact mitochondria and targeted outer membrane proteins exposed to the cytosol, such as TOM70. Swelling the mitochondria with a hypotonic buffer disrupted the outer mitochondrial membrane but left the inner membrane intact, resulting in the cleavage of intermembrane space proteins like SMAC. Lysis with Triton X-100 caused the cleavage of all mitochondrial proteins including matrix proteins like HSP60. Similar to TOM70, WSB2 was cleaved by Protease K digestion in intact mitochondria preparation (**Figure 1M**), supporting its classification as a mitochondrial outer membrane protein.

Collectively, these data indicate that WSB2 specifically interacts with a subset of BCL-2 family proteins on the outer membrane of the mitochondria.

$CRL5^{WSB2}$ E3 ubiquitin ligase complex mediates the ubiquitin-proteasomal degradation of NOXA

WSB2 was co-purified with CRL5 complex components (RBX2, CUL5, ELOB, and ELOC), confirming that WSB2 is a potential CRL5 adaptor (**Figure 1D**). We next investigated whether WSB2 controls the protein stability of its interacting BCL-2 family proteins. Overexpression of WSB2 markedly reduced the levels of co-expressed NOXA in a dose-dependent manner, while other examined BCL-2 family proteins showed minimal or no impact (**Supplementary Figure 1D**). Furthermore, depletion of WSB2 through shRNA-mediated knockdown (KD) or CRISPR/Cas9-mediated knockout (KO) in prostate cancer C4-2B cells or liver cancer Huh-7 cells led to a marked increase in the steady-state levels of endogenous NOXA, without affecting other BCL-2 family proteins examined (**Figure 2A-C, Supplementary Figure 2A, B**). Therefore, our main focus in this study was to investigate the impact of WSB2 on the stability of NOXA. We demonstrated that the proteasome inhibitor MG132 completely reversed the effect of WSB2 on NOXA protein levels, while WSB1 had no effect on NOXA expression levels (**Figure 2D**). WSB2 contains a C-terminal SOCS box consisting of the BC box and the Cullin 5 (CUL5) box, which interact with Elongin B/C and CUL5, respectively[10]. To investigate the roles of these domains, we generated two WSB2 mutants in which the BC box or CUL5 box was

deleted, respectively (**Supplementary Figure 1E**). Strikingly, WSB2-BCM or CULM mutant failed to decrease NOXA protein levels (**Figure 2E**). Furthermore, reintroduction of the WSB2 mutant (BCM, CULM) into WSB2-KO cells was unable to reverse the accumulation of NOXA protein caused by WSB2 deficiency (**Figure 2F**). Depletion of CRL5 complex components (RBX2, CUL5, ELOB, or ELOC) by siRNAs in C4-2B cells also resulted in a marked increase in NOXA protein levels (**Figure 2G**), indicating that the assembly of the $CRL5^{WSB2}$ complex is necessary for NOXA degradation. The half-life of NOXA was notably prolonged in WSB2-KO cells (**Figure 2H**, **I**). Additionally, the mRNA levels of NOXA were even reduced in WSB2-KO cells compared to parental cells, likely to counteract the accumulation of NOXA protein (**Figure 2J**). We also found that WSB2-WT, but not the BCM or CULM mutant, could promote polyubiquitination of NOXA (**Figure 2K**, **L**). By employing linkage-specific K48/K63-Ub mutants, we found that ubiquitinated NOXA primarily consisted of K48-Ub linkages, which is consistent with the expectation that K48-Ub linkage serves as the canonical signal for proteasomal degradation (**Figure 2M**). Conversely, the levels of endogenous ubiquitinated NOXA were diminished in WSB2-KO cells compared to parental cells (**Figure 2N**).

Collectively, these data indicate that the $CRL5^{WSB2}$ complex mediates the ubiquitin-proteasomal degradation of NOXA.

The C-terminal region of NOXA is crucial for WSB2-mediated NOXA degradation

Along with the BC-box and CUL5 box, WSB2 contains five WD repeats that typically serve as protein-protein interaction modules. We generated deletion mutants to determine the region responsible for binding to NOXA, and surprisingly found that WSB's SOCS box, rather than the WD repeats, is required for its interaction with NOXA (**Figure 3A, B**). Deletion of this region abolished WSB2-mediated degradation and ubiquitination of NOXA (**Figure 3C, D**). Reciprocally, we investigated the region in NOXA that is necessary for WSB2 binding. By generating a series of NOXA deletion mutants and conducting co-IP assays, we found that the C-terminal region (40-54 aa) of NOXA mediates its binding to WSB2 (**Figure 3E-G**). This region contains a mitochondrial-targeting domain (MTD)[24]. Mutation of key residues in this domain (5A mutant) eliminated the interaction between NOXA and WSB2. In contrast,

mutation of key residues in the BH3 domain (3E mutant) did not alter the interaction between NOXA and WSB2 (**Figure 3H**). The NOXA-5A mutant was resistant to WSB2-mediated degradation and ubiquitination (**Figure 3I, J**), and had a longer half-life compared to NOXA-WT (**Figure 3K, L**). NOXA contains three lysine residues that can be attached by ubiquitin[25]. By mutating these lysine residues to arginine, we found that WSB2-mediated NOXA ubiquitination was completely abolished, although this mutant (KR) exhibits a comparable WSB2-binding capacity to NOXA-WT (**Figure 3H**, **J**), indicating that these residues function as ubiquitin attachment sites targeted by the $CRL5^{WSB2}$ complex. Furthermore, incubating cell lysates with a C-terminal NOXA peptide (40-54 aa) before conducting co-IP assays resulted in a dose-dependent reduction in the WSB2-NOXA interaction (**Figure 3M**). Based on this, we hypothesized that transduction of the C-terminal NOXA peptide into cells could competitively inhibit WSB2-mediated NOXA degradation. To efficiently deliver this peptide into cells, we synthesized a fusion peptide in which the C-terminal peptide was connected to the cell-penetrating poly-arginine (R8) sequence. Treatment of cells with this fusion peptide dose-dependently increased endogenous NOXA protein levels in C4-2B and Huh-7 cells (**Figure 3N**).

Collectively, these data indicate that the C-terminal region of NOXA is crucial for its interaction with WSB2 and indispensable for WSB2-mediated NOXA degradation.

Co-inhibition of WSB2 and anti-apoptotic BCL-2 family proteins causes synthetic lethality via apoptotic cell death

Despite the strong accumulation of NOXA protein in WSB2-deficient cells, we did not observe obvious spontaneous apoptosis during daily cell culture. This indicated that NOXA upregulation alone may not be sufficient to trigger spontaneous apoptosis. Consequently, we investigated whether co-depletion of an anti-apoptotic BCL-2 family protein would synergistically induce apoptosis in WSB2-deficient cells. Stable cell lines were generated in which BCL-XL or MCL-1 was depleted by shRNAs, followed by further depletion of WSB2 with siRNAs. As shown in **Figure 4A-D**, co-depletion of BCL-XL/WSB2 or MCL-1/WSB2 pairs resulted in substantial apoptosis, as evidenced by Western blot (WB) analysis detecting

caspase cleavage and flow cytometry detecting early apoptotic markers. The E3 ubiquitin ligase MARCH5 co-exists with WSB2 in a functional module (**Figure 1B**), and previous studies have shown that depletion of MARCH5 sensitizes cells to MCL-1 inhibitors or BCL-2/BCL-XL inhibitors[18, 26, 27]. Consistently, we observed that co-depletion of MARCH5/WSB2 also induced substantial apoptosis (**Figure 4E, F**).

Alternatively, we employed a pharmacological approach to inhibit anti-apoptotic BCL-2 family proteins. ABT-737 is a small molecule drug that inhibits BCL-2 and BCL-XL, while AZD5991 is a small molecule drug that inhibits MCL-1. Either ABT-737 or AZD5991 caused only moderate apoptosis in parental C4-2B or Huh-7 cells. However, these drugs induced substantial apoptosis in WSB2-deficient cells (Figure **4G-J**, **Supplementary Figure 3A, B**). In addition to direct inhibitors of the BCL-2 family proteins, inhibitors of cyclin-dependent kinase 9 (CDK9) can indirectly target MCL-1 by suppressing the transcriptional activation of MCL-1 mRNAs[28]. Indeed, we found that the CDK9 inhibitor BAY-1143572 induced moderate apoptosis in parental cells but induced substantial apoptosis in WSB2-deficient cells (**Figure 4K, L**).

Collectively, these data indicate that WSB2 shows synthetic lethality with anti-apoptotic BCL-2 family proteins in cancer cells.

The anti-apoptotic function of WSB2 is primarily reliant on NOXA downregulation

We investigated to determine whether WSB2 plays a role in restricting apoptosis by destabilizing the NOXA protein. As shown in **Figure 5A-D**, reducing NOXA expression through shRNA knockdown in WSB2-deficient C4-2B or Huh-7 cells largely, though not completely, reversed the substantial apoptosis induced by ABT-737 treatment. Likewise, knockdown of NOXA in WSB2-deficient C4-2B cells largely reversed the apoptosis triggered by MCL-1 inhibitor AZD5591 (**Figure 5E, F**). Moreover, we demonstrated that treatment with the C-terminal NOXA peptide sensitized Huh-7 cells to ABT-737-induced apoptosis (**Figure 5G, H**). In xenograft tumor assays, we observed that the C-terminal NOXA peptide or ABT-737 treatment exhibited moderate reductions in tumor growth. Strikingly, co-administration of the C-terminal NOXA peptide and ABT-737 produced significantly

synergetic inhibitory effects on Huh-7 tumors (**Figure 5I, J**).

Collectively, these data indicate that WSB2 deficiency-induced hypersensitivity to BCL-2 family protein inhibitors was at least in part, caused by NOXA accumulation.

Wsb2 knockout mice are more susceptible to apoptosis triggered by BCL-2 family protein inhibitors

To gain deeper insights into the physiological roles of WSB2 in apoptosis *in vivo*, we established a Wsb2 knockout mouse model (**Supplementary Figure 4A**). Homozygous Wsb2$^{-/-}$ knockout mice were observed to be born at Mendelian ratios and exhibited a normal lifespan with no apparent morphological or behavioral abnormalities (**Supplementary Figure 4B, C**). Although some Wsb2$^{-/-}$ mice displayed reduced body size after birth, their adult size generally matched that of wild-type mice. At week 4, we collected multiple mouse tissues, including heart, liver, lung, kidney, and brain. WB analyses demonstrated varying degrees of upregulation in NOXA proteins in the tissues of Wsb2$^{-/-}$ mice compared to wild-type mice. A strong upregulation of NOXA proteins were observed in the liver and heart tissues of Wsb2$^{-/-}$ mice, but not in lung, kidney, and brain tissues, indicating WSB2 modulate NOXA protein levels in a tissue-specific manner. However, the protein levels of caspase 3, 7, and 9 in these tissues were similar between Wsb2$^{-/-}$ mice and wild-type mice (**Supplementary Figure 4D**). Immunofluorescence and WB analyses of heart and liver tissues revealed that cleaved caspases were nearly undetectable in both wild-type and Wsb2$^{-/-}$ mice (**Figure 6A-E**). Consistent with the results from *in vitro* cell culture, Wsb2 deletion alone was insufficient to induce significant apoptosis in mouse organs. We then examined whether pharmacological inhibition of anti-apoptotic BCL-2 family proteins in Wsb2$^{-/-}$ mice would induce substantial apoptosis at the organ level. To test this hypothesis, we utilized ABT-199 (Venetoclax), a highly specific BCL-2 inhibitor. Immunofluorescence and WB analyses of heart and liver tissues showed the presence of obvious cleaved caspases, cleaved PARP1, and TUNEL positive cells in ABT-199-treated Wsb2$^{-/-}$ mice, but not in wild-type mice (**Figure 6A-E, Supplementary Figure. 5A-I**). Furthermore, we isolated primary mouse hepatocytes and exposed them to ABT-199. Consistent with the *in vivo* treatment, *in vitro* cultured Wsb2$^{-/-}$

mouse hepatocytes exhibited increased susceptibility to ABT-199-triggered apoptosis (**Figure 6F**). To assess whether the cardiac injury was caused by ABT-199 treatment, we measured the levels of several cardiac enzyme markers, including CK (creatine kinase), CK-MB (creatine kinase isoenzyme MB), α-HBDH (α-hydroxybutyrate dehydrogenase), and LDH (lactate dehydrogenase) in serum. As shown in **Figure 6G**, ABT-199 administration led to a significant elevation in the levels of these cardiac enzymes in Wsb2$^{-/-}$ mice, whereas no such effect was observed in wild-type mice. This suggested that simultaneous inhibition of Wsb2 and Bcl-2 resulted in heart injury, potentially due to uncontrolled apoptosis in cardiomyocytes.

To investigate whether the anti-apoptotic function of Wsb2 is primarily reliant on mouse NOXA, we isolated mouse embryonic fibroblasts (MEFs). NOXA protein levels were markedly upregulated in Wsb2$^{-/-}$ MEFs compared to wild-type MEFs (**Figure 6H**). Moreover, reducing the expression of NOXA through shRNA-mediated knockdown in Wsb2$^{-/-}$ MEFs largely reversed the substantial apoptosis induced by ABT-199 treatment (**Figure 6I**).

Collectively, these data indicate that WSB2-mediated NOXA destabilization is evolutionally conserved and this regulatory axis is critical for maintaining tissue homeostasis.

WSB2 is overexpressed in several human cancer types

Given the intriguing anti-apoptotic role of WSB2, it is worthwhile to investigate whether WSB2 expression is altered in human cancers. To address this, we analyzed RNA-sequencing (RNA-seq) data from the TCGA cancer cohorts. Remarkably, WSB2 mRNA expression was found to be significantly elevated in the majority of cancer types, including prostate adenocarcinoma (PRAD)and liver hepatocellular carcinoma (LIHC) (**Figure 7A**). Further analysis of the TCGA PRAD cohort revealed a positive correlation between WSB2 mRNA expression and several clinical parameters, including Gleason score (**Figure 7B**), pathological stage (**Figure 7C**), and clinical stage (**Figure 7D**), and nodal metastasis status (**Figure 7E**). Similarly, in the TCGA LIHC cohort, WSB2 mRNA expression showed positive correlations with clinical stage (**Figure 7F**), pathological grade (**Figure 7G**), and nodal metastasis status (**Figure 7H**). Furthermore, survival analysis indicated that high WSB2 expression was significantly correlated with shorter overall survival (OS) in the TCGA LIHC

cohort, but not in the PRAD cohort (**Figure 7I, J**). To validate these findings, we performed immunohistochemistry (IHC) analysis using WSB2-specific antibodies after confirming their specificity (**Supplementary Figure 4C**). Notably, IHC analysis of a PRAD tissue microarray revealed a positive correlation between WSB2 protein expression and Gleason score (**Figure 7K, L**). IHC analysis of a LIHC tissue microarray revealed a positive correlation between WSB2 protein expression and clinical grade (**Figure 7K, L**). At last, we also noticed a higher expression of WSB2 in sorafenib-resistant LIHC patients as compared to sorafenib-sensitive patients by analyzing two publicly available RNA-seq datasets (**Figure 7M, N**).

Collectively, these data suggest that WSB2 expression is abnormally elevated in certain cancer types and may be associated with increased cancer aggressiveness, therapeutic resistance, and decreased overall survival in those types.

Discussion

The WSB2 protein has been identified in several large-scale proteome mapping analyses as being co-purified from the CUL5 scaffold complex[29, 30]. With the presence of a SOCS box in its protein sequence, WSB2 is believed to serve as a receptor for substrates, assisting in their recognition by the CRL5 E3 ubiquitin ligase complex. Its close paralog, WSB1, is induced by hypoxia and can form a $CRL5^{WSB1}$ complex that promotes cancer metastasis by inducing VHL degradation[31]. Additionally, the $CRL5^{WSB1}$ complex overcomes oncogene-induced senescence by targeting ATM for degradation[32]. However, the physiological substrates of the $CRL5^{WSB2}$ complex have not yet been reported. Nevertheless, prior to our current study, there are several pieces of evidence suggesting that this complex may play a role in regulating cell death, possibly involving BCL-2 family proteins. In a large-scale RNAi screening aimed at understanding cancer dependencies and synthetic lethal relationships, the top correlates of WSB2 co-essentiality were found to be MCL-1, BCL-2, and MARCH5, while the most strongly anti-correlated gene with WSB2 was BAX[33]. Two CRISPR/Cas9 knockout screens also showed strong synthetic relationships between WSB2 and MCL-1, BCL-2, or MARCH5[34, 35]. A comprehensive phenotypic CRISPR-Cas9 screen of the ubiquitin pathway revealed that knockout of CUL5, RBX2, or WSB2 resulted in cells becoming hypersensitive to the CRM1

inhibitor leptomycin[36]. Furthermore, a genome-wide CRISPR inhibition (CRISPRi) screen conducted in lung cancer cells demonstrated that knockout of CUL5, RBX2, or UBE2F (a specific E2 for CRL5 E3s) caused cells to become hypersensitive to a CDK9 inhibitor or MCL-1 inhibitor[28]. By connecting the dots from these studies, our findings provide a comprehensive scenario. We have shown that WSB2 can assemble an active $CRL5^{WSB2}$ complex, which mediates the ubiquitination and proteasomal turnover of NOXA, maintaining its low-level expression under basal conditions. WSB2 deficiency leads to a remarkable accumulation of NOXA, but it alone is not sufficient to trigger spontaneous apoptosis. This is consistent with previous studies showing that enforced expression of NOXA alone is ineffective at triggering apoptosis in various cell types[37, 38]. Striking when combined with genetic or pharmacological inhibition of anti-apoptotic BCL-2 family proteins, massive apoptosis occurs in WSB2-deficient cells (**Figure 8**). However, it is important to note that knockdown of NOXA expression in WSB2-deficient cells largely, but not completely, reverses the massive apoptosis induced by BCL-2 family protein inhibitors, implying that WSB2 may also modulate apoptosis through other unidentified targets. Indeed, WSB2 interacts with multiple BCL-2 family proteins (MCL-1, BCL-2, BCL-XL, and BAD) (**Figure 1F-J**). Although WSB2 does not alter their turnover, it is still possible that WSB2 modulates the apoptotic function of these proteins through direct binding. Further investigation is warranted to fully elucidate the molecular mechanisms underlying WSB2-mediated anti-apoptotic function. Lastly，it would also be interesting to explore whether there are any upstream signals capable of overriding WSB2-mediated NOXA destabilization under specific stress conditions.

In the current study, our focus was primarily on investigating the *in vivo* anti-apoptotic function of WSB2. Thus, we did not extensively characterize the potential morphological and behavioral abnormalities in $Wsb2^{-/-}$ mice. However, recent large-scale mouse phenotype analyses conducted by the International Mouse Phenotyping Consortium (IMPC) have reported abnormalities in tooth morphology, locomotor activity, retina, heart, osmotic and electrolyte balance, as well as male infertility in $Wsb2^{-/-}$ mice[39]. It remains unclear whether these abnormalities are a result of NOXA accumulation and subsequent dysregulated apoptosis. Generating Wsb2/NOXA double knockout mice would be beneficial in determining

375 whether these abnormalities can be reversed by further ablating NOXA expression. Despite
376 the fact that WSB2 is upregulated in various types of cancer and exhibits a strong
377 anti-apoptotic function, which makes it a promising target for cancer therapy, it is crucial to
378 comprehensively understand the downstream substrates regulated by the $CRL5^{WSB2}$ complex.
379 This understanding will help us evaluate the potential effects of pharmacological inhibition of
380 WSB2, as it may lead to the dysregulation of other substrates and undesirable side effects.
381 Since its initial discovery as a novel phorbol-12-myristate13-acetate (PMA) responsive gene
382 in T cells, and subsequently as a transcriptional target of the genotoxic response regulator p53,
383 NOXA has emerged as a critical player in regulating cell death pathways in various cell types
384 under stressed conditions[40]. Notably, NOXA is implicated in fine-tuning apoptosis induction in
385 cancer cells treated with genotoxic anticancer drugs, including paclitaxel (a microtubule
386 targeting agent), bortezomib (a proteasome inhibitor), and MLN4924 (a CRL E3 ligase
387 inhibitor)[40]. These different agents engage distinct mechanisms, such as transcriptional
388 activation or protein stabilization, to upregulate NOXA protein levels and initiate apoptotic cell
389 death[40]. The half-life of NOXA protein was very short, as it undergoes ubiquitin-proteasomal
390 degradation mediated by the addition of ubiquitin to specific lysine residues[10]. In mantle cell
391 lymphoma (MCL) cell lines, despite high NOXA transcript levels, low NOXA protein expression
392 is observed due to rapid protein degradation[41]. Similarly, paradoxical downregulation of NOXA
393 protein is observed in Cushing's disease (CD) adenomas, despite transcriptional upregulation
394 caused by recurrent promoter hypomethylation[42]. These observations suggest that certain
395 tumor cells may exploit pathways to accelerate NOXA degradation, thus suppressing
396 apoptosis. The elevated NOXA mRNA levels observed in tumor cells may potentially serve as
397 a compensatory mechanism to counteract the reduction in NOXA protein levels. Previous
398 studies have only partially characterized the ubiquitin-proteasomal degradation of NOXA,
399 showing that UBE2F, in conjunction with RBX2, induces CUL5 neddylation, leading to CRL5
400 E3 activation and subsequent NOXA degradation[28]. In lung cancer tissues, high levels of
401 UBE2F and CUL5 correlate with reduced NOXA levels and poorer survival in patients.
402 However, the specific CRL5 substrate receptor responsible for NOXA destabilization has yet to
403 be identified[43]. In our study, we identified WSB2 as the substrate receptor for NOXA, thereby

shedding light on its role in regulating NOXA turnover. Further investigation is needed to determine whether WSB2 dysregulation is responsible for the accelerated protein turnover observed in various cancer types, such as MCL and CD adenomas. It should also be noted that WSB2 only facilitates NOXA destabilization in certain tissues/organs, such as heart, and liver, in mouse models. It is not surprising that a specific substrate can be targeted by multiple E3 ubiquitin ligases. A previous study has indicated that treatment with a proteasome inhibitor could further increase NOXA protein levels in CUL5 knockout cells, suggesting that the turnover of NOXA can be regulated by additional ubiquitin ligases apart from the CRL5 E3 [28]. In fact, the RING domain containing E3 ubiquitin ligases MARCH5 have been reported to mediate NOXA degradation [18-20, 26, 27]. Further investigation is needed to determine which E3 ubiquitin ligase(s) play the predominant roles in specific tissues/organs or types of cancer.

Although bortezomib and MLN4924 have proven effective in stabilizing the NOXA protein and promoting NOXA-dependent apoptosis, their broad inhibition of the proteasome or all CRL E3 ligases, respectively, inevitably leads to side effects. In this study, we have conducted preliminary investigations on the use of a competitive peptide to effectively inhibit the binding of WSB2 and NOXA, resulting in the accumulation of NOXA proteins and increased sensitivity to ABT-737. In the future, other potential therapeutic strategies can be explored, such as designing PROTAC molecules specifically for degrading WSB2 or developing small molecules to disrupt the interaction between WSB2 and NOXA. Extensive research is needed to determine the safety and efficacy of these approaches in preclinical cancer models.

Materials and methods

Acquisition and analysis of DepMap and drug sensitivity datasets

Gene co-dependencies were determined using the Achilles datasets (https://depmap.org/portal/). The Achilles dataset contains dependency scores from genome-scale essentiality screens scores of 789 cell lines. As a measure of co-dependency, the Pearson's correlation coefficient of essentiality scores was computed for all gene pairs. GO analysis for the top 500 genes co-dependent-with WSB2 was performed using PANTHER to

search enriched biological processes and pathways. Co-essential module assigns of cellular component: Bcl-2 family protein complex were obtained from a previously published dataset(Gene co-dependency (https://mitra.stanford.edu/bassik/michael/cluster_heatmaps/)[17]. To identify genetic and pharmacologic perturbations that induce similar effects on cell viability, a Web tool, DepLink (https://shiny.crc.pitt.edu/deplink/) was used[21].

Cell line, cell culture, transfection, and lentiviral infection

293T, HeLa, C4-2B, and Huh-7 cells were obtained from the American Type Culture Collection (ATCC). 293T, HeLa and Huh-7 cells were maintained in Dulbecco's modified Eagle's medium (DMEM) supplemented with 10% FBS. C4-2B cells were maintained in RPMI1640 medium supplemented with 10% FBS. We routinely perform DNA fingerprinting and PCR to verify the authenticity of the cell lines and to ensure they are free of mycoplasma infection. We conducted transient transfection using EZ Trans (Shanghai Life-iLab Biotech). For lentiviral transfection, we transfected pLKO shRNA KD and virus-packing constructs into 293 T cells. The viral supernatant was collected after 48 h. The cells were then infected with the viral supernatant in the presence of polybrene (8 μg/ml) and selected in growth media containing puromycin (1.5 μg/ml). The gene-specific shRNA or siRNA sequences can be found in **Supplementary Table 4**.

Antibodies, chemicals, and kits

The information of antibodies, chemicals, and kits used in this study is listed in **Supplementary Table 5, 6.**

Plasmid construction

The plasmids used for transient overexpression were constructed using the pCMV-FLAG/Myc vector (Clontech). Point and deletion mutants were engineered utilizing the KOD-Plus-Mutagenesis Kit (TOYOBO) following the manufacturer's instructions. Single-guide RNAs (sgRNAs) targeting WSB2 (http://crispr.mit.edu) were subcloned into the pSpCas9(BB)-2A-Puro (PX459) vector for gene knockout (KO). Short hairpin RNAs (shRNAs)

targeting WSB2 or BCL-2 family proteins were subcloned into the pLKO.1 puro vector (Addgene) for gene KD. The sequences of gene-specific sgRNAs and shRNAs are listed in **supplementary table 4**.

Isolation of nucleic, cytoplasmic, and mitochondrial fractions

HeLa cells were prepared for nuclear, cytoplasmic, and mitochondrial extraction by density-gradient centrifugation. Briefly, HeLa cells were washed three times with PBS. Then the cells are suspended by using hypotonic solution (140 mM KCl, 10 mM EDTA, 5 mM MgCl2, 20 mM HEPES (pH 7.4), and the protease inhibitor). Then 5 × 106 HeLa cells were ground with a glass homogenizer in an ice bath for 25 strokes. Nuclear, cytoplasmic, and mitochondrial fractions were separated through differential centrifugation (800×g, 10 min, 4°C and 12,000×g, 35 min, 4°C). The supernatant (cytoplasmic fraction) and pellet (mitochondrial fraction) were collected, and the pellet was further washed with wash buffer (800 mM KCl, 10 mM EDTA, 5 mM MgCl2, and 20 mM HEPES (pH 7.4), and the protease inhibitor) for three times and yield the final mitochondrial fraction. To confirm that pure extracts were obtained, the mitochondrial, nuclear, and cytoplasmic fractions were separated by SDS-PAGE, and the presence of mitochondrial VDAC1, BCL2, nuclear Histone H3, and cytoplasmic GAPDH was detected by Immunoblot.

Isolation of submitochondrial fractions

Six mitochondrial fraction samples were divided into three groups, with two samples in each group. The first group was resuspended in 300 μl of homogenization buffer, the second group in 300 μl of hypotonic swelling buffer (10 mM HEPES/KOH, pH 7.4, 1 mM EDTA), and the third group in 300 μl of homogenization buffer supplemented with 0.5% (V/V) Triton X-100, followed by a 10-min incubation on ice. Subsequently, one sample from each group was exposed to proteinase K (70 μg/ml) for 20 min on ice, while the other sample was kept untreated as a control. Following the treatments, mitochondrial proteins were precipitated using 300 μl of 30% TCA (W/V) and incubated on ice for 10 min. The proteins were collected by centrifugation at 18,000 g for 10 min at 4°C, washed with 1 ml of 100% ethanol, and centrifuged again. The

resulting pellets were dissolved in 100 μl of SDS Lysis Buffer, boiled at 105°C for 8 min, and subjected to WB analyses.

CRISPR-Cas9 mediated gene KO cell lines

C4-2B or Huh-7 cells were plated and transfected with PX459 plasmids overnight. 24 h after transfection, 1 μg/ml puromycin was used to screen cells for three days. Living cells were seeded in 96-well plate by limited dilution to isolate monoclonal cell line. The knock out cell clones are screened by WB and validated by Sanger sequencing. Sequences of gene-specific sgRNAs are listed in **Supplementary Table 4**.

RT-qPCR assays

Total RNA from cells were extracted by using TRIzol reagent (TIANGEN), followed by reverse transcription into cDNA using the HiScript III First Strand cDNA Synthesis Kit (Vazyme). The synthesized cDNAs were then subjected to PCR amplification using ChamQ SYBR qPCR Master Mix (Vazyme) in CFX Real-Time PCR system (Bio-Rad). The relative mRNA levels of DDHD2 were quantified using the $2^{-\Delta\Delta CT}$ method with normalization to GAPDH. The primer sequences are listed in the **Supplementary Table 4**.

***In vivo* ubiquitination assays**

293T cells were transfected with HA-ubiquitin and indicated constructs. After 36 h, cells were treated with MG132 (30 μM) for 6 h and then lysed in 1% SDS buffer (Tris [pH 7.5], 0.5 mM EDTA, 1 mM DTT) and boiled for 10 min. For immunoprecipitation, the cell lysates were diluted 10-fold in Tris-HCL buffer and incubated with anti-NOXA or IgG-conjugated beads (Sigma) for 4 h at 4 °C. The bound beads are then washed four times with BC100 buffer (20 mM Tris-Hcl, pH 7.9,100 mM NaCl,0.2 mM EDTA, 20% glycerol) containing 0.2% Triton X-100. The proteins were eluted with FLAG peptide for 2 h at 4°C. The ubiquitinated form of NOXA was detected by WB using anti-HA antibody.

IF and confocal microscopy

HeLa cells were seeded on glass coverslips in 12-well plates and harvested at 70% confluence. The cells were washed with PBS and fixed with 4% paraformaldehyde in PBS. After permeabilization with 0.3% Triton X-100 for 5 min and then in the blocking solution (PBS plus 5% donkey serum), for 1h at room temperature (RT). The cells were then incubated with primary antibodies at 4 °C for overnight. After washing with PBST buffer, fluorescence-labelled secondary antibodies were applied. DAPI was utilized to stain nuclei. The glass coverslips were mounted on slides and imaged using a confocal microscope (LSM880, Zeiss) with a 63*/1.4NA Oil PSF Objective. Quantitative analyses were performed using ImageJ software.

For mouse tissues staining, the mouse tissues were isolated from mice after perfusion with 0.1 M PBS (pH7.4) and fixed for 3 days with 4% PFA at 4 °C. The tumor tissues were then placed in 30% sucrose solution for 5 days for dehydration. The tumors were embedded into the OCT block and frozen for cryostat sectioning. Cryostat sections (45-μm thick) were washed with PBS, and then incubated in blocking solution (PBS containing 10% goat serum, 0.3% Triton X-100, pH7.4) for 2h at RT. The samples were stained with primary antibodies overnight at 4 °C, after washing with PBST buffer, fluorescence-labelled secondary antibodies were applied at RT for 2h. DAPI was utilized to stain nuclei. The sections were then sealed with an anti-fluorescence quencher. The samples were visualized and imaged using a confocal microscope (LSM880, Zeiss) with a 63*/1.4NA Oil PSF Objective. Quantitative analyses were performed using ImageJ software.

Apoptosis assays

Annexin V-FITC (Fluorescein isothiocyanate) and propidium iodide (PI) double staining (Dojindo) were used to detect the apoptosis rates. The cells were cultured in six-well plates at a density of 1.2 × 105/well and allowed to adhere to culture plate overnight. Then the medium was replaced with fresh medium containing indicated drugs for a certain time. The cells were then trypsinized by EDTA-free trypsin and washed twice with cold PBS. Aliquots of the cells were resuspended in 100 μl of binding buffer and stained with 5 μl of annexin V-FITC and 5 μl of PI working solution for 15 min at RT in the dark. All flow cytometry analyses were carried out using a Fortessa flow cytometer (BD Bioscience). The subsequent data analysis was

conducted using FlowJo software.

Generation and breeding of Wsb2 KO mice

Mice with murine Wsb2 KO were designed and generated from Shanghai Model Organisms Center (Shanghai, China). In brief, CRISPR/Cas9 system were microinjected into the fertilized eggs of C57BL/6JGpt mice. Fertilized eggs were transplanted to obtain positive F0 mice which were confirmed by PCR and sequencing. A stable F1 generation mouse model was obtained by mating positive F0 generation mice with C57BL/6JGpt mice. The genotype of F1 mice was identified by PCR and confirmed by sequencing. The sequences used for CRISPR-Cas9 editing and the primers used for genotyping are listed in **Supplementary Table 4**.

Mice were maintained under a 12 h/12 h light/dark cycle at 22–25 °C and 40–50% humidity with standard food and water available ad libitum. All procedures for animal care and animal experiments were carried out in accordance with the guidelines of the Care and Use of Laboratory Animals proposed by Institute of Development Biology and Molecular Medicine and Shanghai Municipality, PR China. The male C57BL/6JGpt mice (8 months old) were divided into 2 groups ($Wsb2^{+/+}$ and $Wsb2^{-/-}$; n=5/group), each group was given by gavage of ABT-199 (100 mg/kg per day) or vehicle (10% β-cyclodextrin) for one week. Then, we collect blood samples from the tail vein of mice before and after oral administration to measure indicators of myocardial zymogram using an Olympus AU640 automatic biochemical analyzer (Olympus).

MEFs generation and immortalization

Timed pregnant female mice at embryonic day 12.5 to 14.5 were sacrificed, and the embryos were carefully dissected to remove the cerebrum, internal organs, and limbs. The remaining tissues were cut into small pieces and treated with trypsin-EDTA (0.25%) for 10 min at 37 °C. The trypsin was neutralized with DMEM, a complete medium supplemented with 10 % fetal bovine serum and 1% penicillin/streptomycin. The culture media were changed every 2-3 days until the cells reached confluence. To immortalize MEFs, they were passaged up to approximately 10 times before infection with lentiviral vectors expressing the SV40 large T-antigen. Stable transduction was achieved with puromycin selection. The successful

integration of the immortalizing gene was confirmed through Sanger sequencing and WB analysis.

Mouse tumor implantation

All experimental protocols were approved in advance by the Ethics Review Committee for Animal Experimentation of Fudan University. 4–6-week-old male BALB/c nu/nu mice obtained from SLAC Laboratory Animal Co., Ltd. were bred and maintained in our institutional pathogen-free mouse facilities. Mice were randomly divided into 4 groups (n=6/group): vehicle (distilled water); ABT-737 (20 mg/kg); R8-C-ter (20 mg/kg); and ABT-737+R8-C-ter. Huh-7 tumors were established by subcutaneously injecting 5 × 106 Huh-7 cells in 100 μl of PBS buffer into the right flank of 6-week-old nude mice. After 1 week, vehicle and indicated drug treatments were administered once daily by intraperitoneal injection (i.p). At the end of 3 weeks, mice were killed and *in vivo* solid tumors were dissected and weighed.

Pan-cancer dataset acquisition and analysis

Pan-cancer gene expression analysis based on tumor and normal samples was derived from the TCGA (transcriptome datasets, http://gepia2.cancer-pku.cn/). Public databases (TCGA) were used to analyze the correlations of WSB2 expression with clinical risk factors. Additional publicly available RNA-seq datasets (GSE104580 and GSE109211) provided for sorafenib-response and sorafenib-non-response HCC patients.

IHC analysis

A total of 84 patients with localized PRAD, who underwent radical prostatectomy between January 2007 and July 2014 at Fudan University Shanghai Cancer Center (FUSCC), were included in this study. All the patients underwent regular postoperative reviews and had long-term follow-up data. This study was in accordance with the recommendations of the Research Ethics Committee of FUSCC according to the provisions of the Declaration of Helsinki (as revised in Fortaleza, Brazil, October 2013). The protocol was approved by the Research Ethics Committee of FUSCC. Informed consent for the use of clinical data was

obtained from all the patients recruited in this study. The TMA consist of 29 LIHC patient specimens was obtained from Shanghai Biochip Co., Ltd (Shanghai). To confirm the specificity of the anti-WSB2 antibody, we conducted genetic control for the IHC analysis using an anti-WSB2 antibody in both parental and WSB2 KO C4-2B cells.

Statistical analysis

Statistical analysis was performed using GraphPad Prism (GraphPad Software), and the differences between the two groups were analyzed using one-way analysis of variance (ANOVA) or two-way analysis of variance ANOVA. All data were displayed as means ± S.D. values for experiments conducted with at least three replicates. * represents $p < 0.05$; ** represents $p < 0.01$; *** represents $p < 0.001$, **** represents $p < 0.0001$.

Acknowledgements

The graphical model image was generated by BioRender.com.

Authors' contributions

C.W. conceived the study. D.J., K.C., and J.J. performed the experiments and data analyses. C.W., D.J., K.G., and Y.X. analyzed and interpreted the data. C.W. wrote the manuscript.

Funding

This work was in part supported by the National Natural Science Foundation of China (No. 92357301, 32370726, 91957125 to C.W., 82272992, 91954106, and 81872109 to K.G.; 82270415 to L.W), the State Key Development Programs of China (No. 2022YFA1104200 to C.W), the Natural Science Foundation of Shanghai (No. 22ZR1406600 to C.W.; 22ZR1449200 to K.G, 22ZR1448600 to Y.X), Science and Technology Research Program of Shanghai (No. 9DZ2282100). Open Research Fund of the State Key Laboratory of Genetic Engineering, Fudan University (No. SKLGE-2111 to K.G.), Science and Technology Research Program of Shanghai (No. 9DZ2282100), and Central Guidance on Local Science and Technology Development Foundation (No. 2021ZY0037 to R.M.).

Competing interests

The authors declare no competing interests.

Reference

1. Hanahan, D. & Weinberg, R.A. Hallmarks of cancer: the next generation. *Cell* **144**, 646-674 (2011).
2. Carneiro, B.A. & El-Deiry, W.S. Targeting apoptosis in cancer therapy. *Nat Rev Clin Oncol* **17**, 395-417 (2020).
3. Kale, J., Osterlund, E.J. & Andrews, D.W. BCL-2 family proteins: changing partners in the dance towards death. *Cell Death Differ* **25**, 65-80 (2018).
4. Youle, R.J. & Strasser, A. The BCL-2 protein family: opposing activities that mediate cell death. *Nat Rev Mol Cell Biol* **9**, 47-59 (2008).
5. Cory, S., Roberts, A.W., Colman, P.M. & Adams, J.M. Targeting BCL-2-like Proteins to Kill Cancer Cells. *Trends Cancer* **2**, 443-460 (2016).
6. Wei, A.H. *et al.* Venetoclax plus LDAC for newly diagnosed AML ineligible for intensive chemotherapy: a phase 3 randomized placebo-controlled trial. *Blood* **135**, 2137-2145 (2020).
7. DiNardo, C.D. *et al.* Azacitidine and Venetoclax in Previously Untreated Acute Myeloid Leukemia. *N Engl J Med* **383**, 617-629 (2020).
8. Ploumaki, I. *et al.* Bcl-2 pathway inhibition in solid tumors: a review of clinical trials. *Clin Transl Oncol* **25**, 1554-1578 (2023).
9. Zhao, Y., Xiong, X. & Sun, Y. Cullin-RING Ligase 5: Functional characterization and

659 its role in human cancers. *Semin Cancer Biol* **67**, 61-79 (2020).

660 10. Mahrour, N. *et al.* Characterization of Cullin-box sequences that direct recruitment of
661 Cul2-Rbx1 and Cul5-Rbx2 modules to Elongin BC-based ubiquitin ligases. *J Biol*
662 *Chem* **283**, 8005-8013 (2008).

663 11. Zhang, Y. *et al.* WD repeat and SOCS box containing protein 2 in the proliferation,
664 cycle progression, and migration of melanoma cells. *Biomed Pharmacother* **116**,
665 108974 (2019).

666 12. Ma, L., Zhang, Y. & Hu, F. miR‐28‐5p inhibits the migration of breast cancer by
667 regulating WSB2. *Int J Mol Med* **46**, 1562-1570 (2020).

668 13. Wei, X. *et al.* WSB2 as a target of Hedgehog signaling promoted the malignant
669 biological behavior of Xuanwei lung cancer through regulating Wnt/beta-catenin
670 signaling. *Transl Cancer Res* **9**, 7394-7404 (2020).

671 14. Tsherniak, A. *et al.* Defining a Cancer Dependency Map. *Cell* **170**, 564-576 e516
672 (2017).

673 15. Bayraktar, E.C. *et al.* Metabolic coessentiality mapping identifies C12orf49 as a
674 regulator of SREBP processing and cholesterol metabolism. *Nat Metab* **2**, 487-498
675 (2020).

676 16. Price, C. *et al.* Genome-Wide Interrogation of Human Cancers Identifies EGLN1
677 Dependency in Clear Cell Ovarian Cancers. *Cancer Res* **79**, 2564-2579 (2019).

678 17. Wainberg, M. *et al.* A genome-wide atlas of co-essential modules assigns function to
679 uncharacterized genes. *Nat Genet* **53**, 638-649 (2021).

680 18. Nakao, F. *et al.* Targeting a mitochondrial E3 ubiquitin ligase complex to overcome

681 AML cell-intrinsic Venetoclax resistance. *Leukemia* **37**, 1028-1038 (2023).

682 19. Djajawi, T.M. *et al.* MARCH5 requires MTCH2 to coordinate proteasomal turnover of
683 the MCL1:NOXA complex. *Cell Death Differ* **27**, 2484-2499 (2020).

684 20. Haschka, M.D. *et al.* MARCH5-dependent degradation of MCL1/NOXA complexes
685 defines susceptibility to antimitotic drug treatment. *Cell Death Differ* **27**, 2297-2312
686 (2020).

687 21. Nayak, T. *et al.* DepLink: an R Shiny app to systematically link genetic and
688 pharmacologic dependencies of cancer. *Bioinform Adv* **3**, vbad076 (2023).

689 22. Corsello, S.M. *et al.* Discovering the anti-cancer potential of non-oncology drugs by
690 systematic viability profiling. *Nat Cancer* **1**, 235-248 (2020).

691 23. Iorio, F. *et al.* A Landscape of Pharmacogenomic Interactions in Cancer. *Cell* **166**,
692 740-754 (2016).

693 24. Seo, Y.W. *et al.* The molecular mechanism of Noxa-induced mitochondrial dysfunction
694 in p53-mediated cell death. *J Biol Chem* **278**, 48292-48299 (2003).

695 25. Pang, X. *et al.* The carboxyl-terminal tail of Noxa protein regulates the stability of Noxa
696 and Mcl-1. *J Biol Chem* **289**, 17802-17811 (2014).

697 26. Subramanian, A., Andronache, A., Li, Y.C. & Wade, M. Inhibition of MARCH5 ubiquitin
698 ligase abrogates MCL1-dependent resistance to BH3 mimetics via NOXA. *Oncotarget*
699 **7**, 15986-16002 (2016).

700 27. Arai, S. *et al.* MARCH5 mediates NOXA-dependent MCL1 degradation driven by
701 kinase inhibitors and integrated stress response activation. *Elife* **9** (2020).

702 28. Kabir, S. *et al.* The CUL5 ubiquitin ligase complex mediates resistance to CDK9 and

703 MCL1 inhibitors in lung cancer cells. *Elife* **8** (2019).

704 29. Huttlin, E.L. *et al.* Architecture of the human interactome defines protein communities
705 and disease networks. *Nature* **545**, 505-509 (2017).

706 30. Bennett, E.J., Rush, J., Gygi, S.P. & Harper, J.W. Dynamics of cullin-RING ubiquitin
707 ligase network revealed by systematic quantitative proteomics. *Cell* **143**, 951-965
708 (2010).

709 31. Kim, J.J. *et al.* WSB1 promotes tumor metastasis by inducing pVHL degradation.
710 *Genes Dev* **29**, 2244-2257 (2015).

711 32. Kim, J.J. *et al.* WSB1 overcomes oncogene-induced senescence by targeting ATM for
712 degradation. *Cell Res* **27**, 274-293 (2017).

713 33. McDonald, E.R., 3rd *et al.* Project DRIVE: A Compendium of Cancer Dependencies
714 and Synthetic Lethal Relationships Uncovered by Large-Scale, Deep RNAi Screening.
715 *Cell* **170**, 577-592 e510 (2017).

716 34. DeWeirdt, P.C. *et al.* Genetic screens in isogenic mammalian cell lines without single
717 cell cloning. *Nat Commun* **11**, 752 (2020).

718 35. DeWeirdt, P.C. *et al.* Optimization of AsCas12a for combinatorial genetic screens in
719 human cells. *Nat Biotechnol* **39**, 94-104 (2021).

720 36. Hundley, F.V. *et al.* A comprehensive phenotypic CRISPR-Cas9 screen of the
721 ubiquitin pathway uncovers roles of ubiquitin ligases in mitosis. *Mol Cell* **81**,
722 1319-1336 e1319 (2021).

723 37. Akhtar, R.S. *et al.* BH3-only proapoptotic Bcl-2 family members Noxa and Puma
724 mediate neural precursor cell death. *J Neurosci* **26**, 7257-7264 (2006).

725 38. Shibue, T. *et al.* Differential contribution of Puma and Noxa in dual regulation of
726 p53-mediated apoptotic pathways. *EMBO J* **25**, 4952-4962 (2006).
727 39. da Silva-Buttkus, P. *et al.* Knockout mouse models as a resource for the study of rare
728 diseases. *Mamm Genome* **34**, 244-261 (2023).
729 40. Ploner, C., Kofler, R. & Villunger, A. Noxa: at the tip of the balance between life and
730 death. *Oncogene* **27 Suppl 1**, S84-92 (2008).
731 41. Dengler, M.A. *et al.* Discrepant NOXA (PMAIP1) transcript and NOXA protein levels: a
732 potential Achilles' heel in mantle cell lymphoma. *Cell Death Dis* **5**, e1013 (2014).
733 42. Asuzu, D.T. *et al.* Pituitary adenomas evade apoptosis via noxa deregulation in
734 Cushing's disease. *Cell Rep* **40**, 111223 (2022).
735 43. Zhou, W. *et al.* Neddylation E2 UBE2F Promotes the Survival of Lung Cancer Cells by
736 Activating CRL5 to Degrade NOXA via the K11 Linkage. *Clin Cancer Res* **23**,
737 1104-1116 (2017).
738
739
740
741
742
743
744
745
746

Figure Legends

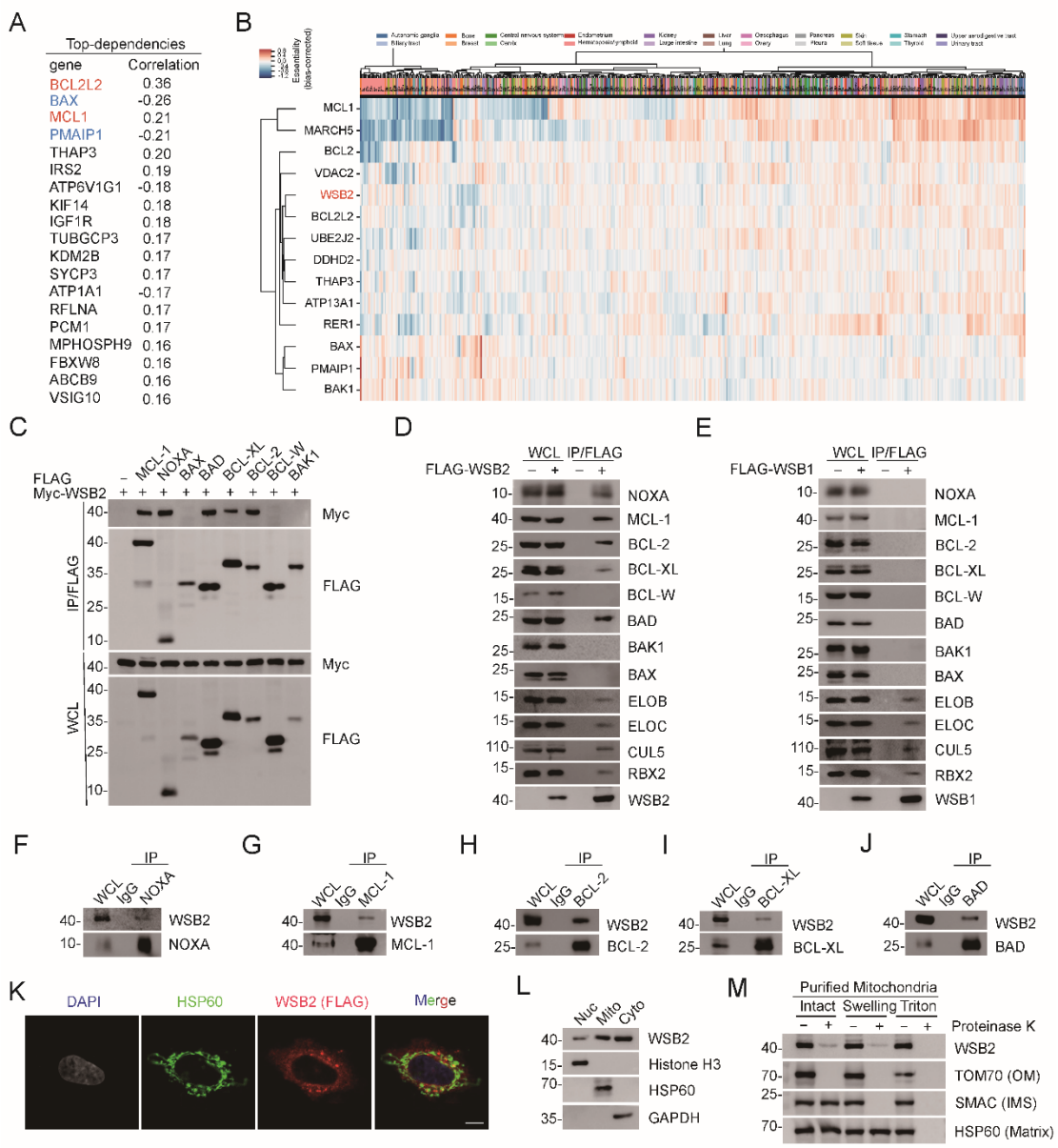

Figure 1. WSB2 interacts with multiple members of BCL-2 family proteins in cells.

(**A**) The top 20 co-dependent genes of WSB2 in Broad's 21Q2 DepMap dataset. Red, anti-apoptotic BCL-2 family proteins. Blue, pro-apoptotic BCL-2 family proteins.

(**B**) A co-essential module containing WSB2 and other BCL-2 family proteins using a dataset of CRISPR screens in 485 cell lines from the Achilles DepMap project. Cellular component: Bcl-2 family protein complex. Molecular function: BH domain binding.

(**C-E**) WB analyses of the indicated proteins in the whole cell lysates (WCL) and co-IP samples of anti-FLAG antibody obtained from 293 T cells transfected with the indicated plasmids.

(**F-J**) WB analyses of the indicated proteins in WCL and co-IP samples of IgG or anti-NOXA

(**F**), anti-MCL-1 (**G**), anti-BCL-2 (**H**), anti-BCL-XL (**I**), or anti-BAD (**J**) antibodies obtained from 293T cells.

(**K**) Representative IF images from HeLa cells transfected with FLAG-WSB2, stained with FLAG (WSB2), HSP60, and DAPI. Scale bar, 20 μm.

(**L**) The cytoplasmic (Cyto), mitochondrial (Mito), and nuclear fractions (Nuc) from HeLa cells were prepared as described in Methods section. Histone H3 (nucleus), GAPDH (cytoplasm), and HSP60 (mitochondria) were used as subcellular fraction markers. WB analyses were performed to detect the indicated proteins in three fractions from HeLa cells.

(**M**) Mitochondria from HeLa cells were purified as intact mitochondria or treated with hypotonic swelling buffer or lysed with Triton X-100 buffer. Different mitochondrial preparations were then digested with or without Proteinase K. WB analyses of the indicated proteins in three fractions were then performed. OM: outer membrane; IMS: intermembrane space.

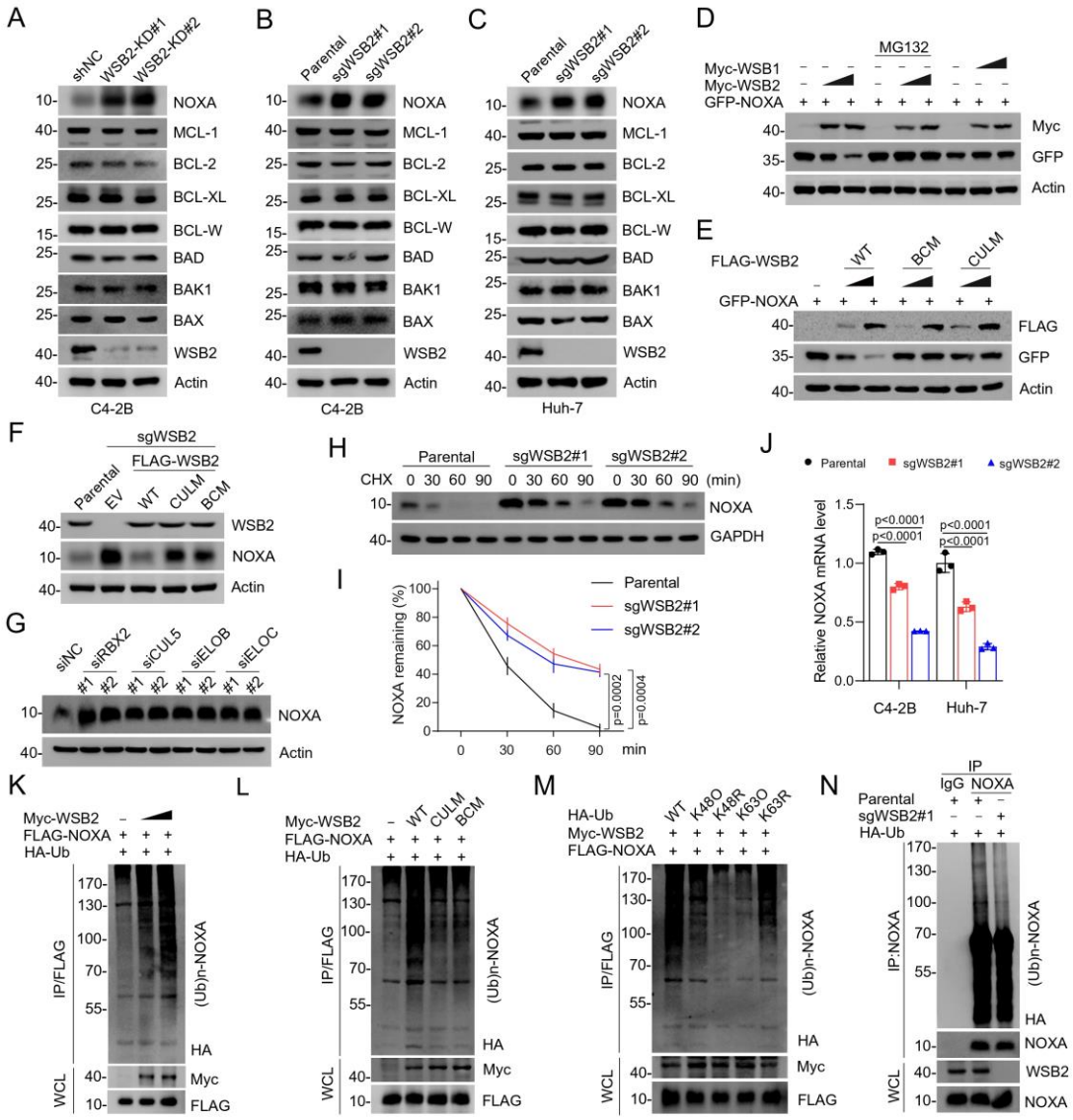

Figure 2. CRL5^{WSB2} E3 ubiquitin ligase complex control NOXA protein turnover.

(**A**) WB analyses of the indicated proteins in the WCL from C4-2B cells infected with lentivirus expressing WSB2-specific shRNA or negative control (NC).

(**B, C**) WB analyses of the indicated proteins in the WCL from parental or WSB KO C4-2B or Huh-7 cells.

(**D**) WB analyses of the indicated proteins in the WCL from 293 T cells transfected with the indicated plasmids for 24 h and treated with DMSO or MG132 (20 μM) for 8 h.

(**E**) WB analyses of the indicated proteins in the WCLs from 293 T cells transfected with the indicated plasmids.

(**F**) WB analyses of the indicated proteins in the WCL from parental or WSB2 KO C4-2B cells stably overexpressing empty vector (EV), WSB2-WT or its mutants.

(**G**) WB analyses of the indicated proteins in the WCL from C4-2B cells transfected with the indicated siRNAs.

(**H, I**) WB analyses of indicated proteins in WCLs of parental and WSB2 KO C4-2B cells treated with cycloheximide (CHX, 50 μg/ml) and harvested at different time points. (**G**) At each time point, the intensity of NOXA was normalized to the intensity of GAPDH and then to the value at 0h. Data are shown as means ± SD (n=3).

(**K-M**) WB analyses of the products of *in vivo* ubiquitination assays performed using WCL from 293T cells transfected with the indicated plasmids and treated with MG132(20 μM).

(**N**) WB analyses of the products of *in vivo* ubiquitination assays. Co-IP using anti-IgG or anti-NOXA antibody in the WCL prepared from parental and WSB2 KO C4-2B cells transfected with HA-Ub for 24 h and treated with MG132(20 μM) for 8 h.

P values are calculated by the Two-way ANOVA test in (**G**) and One-way ANOVA test in (**H**).

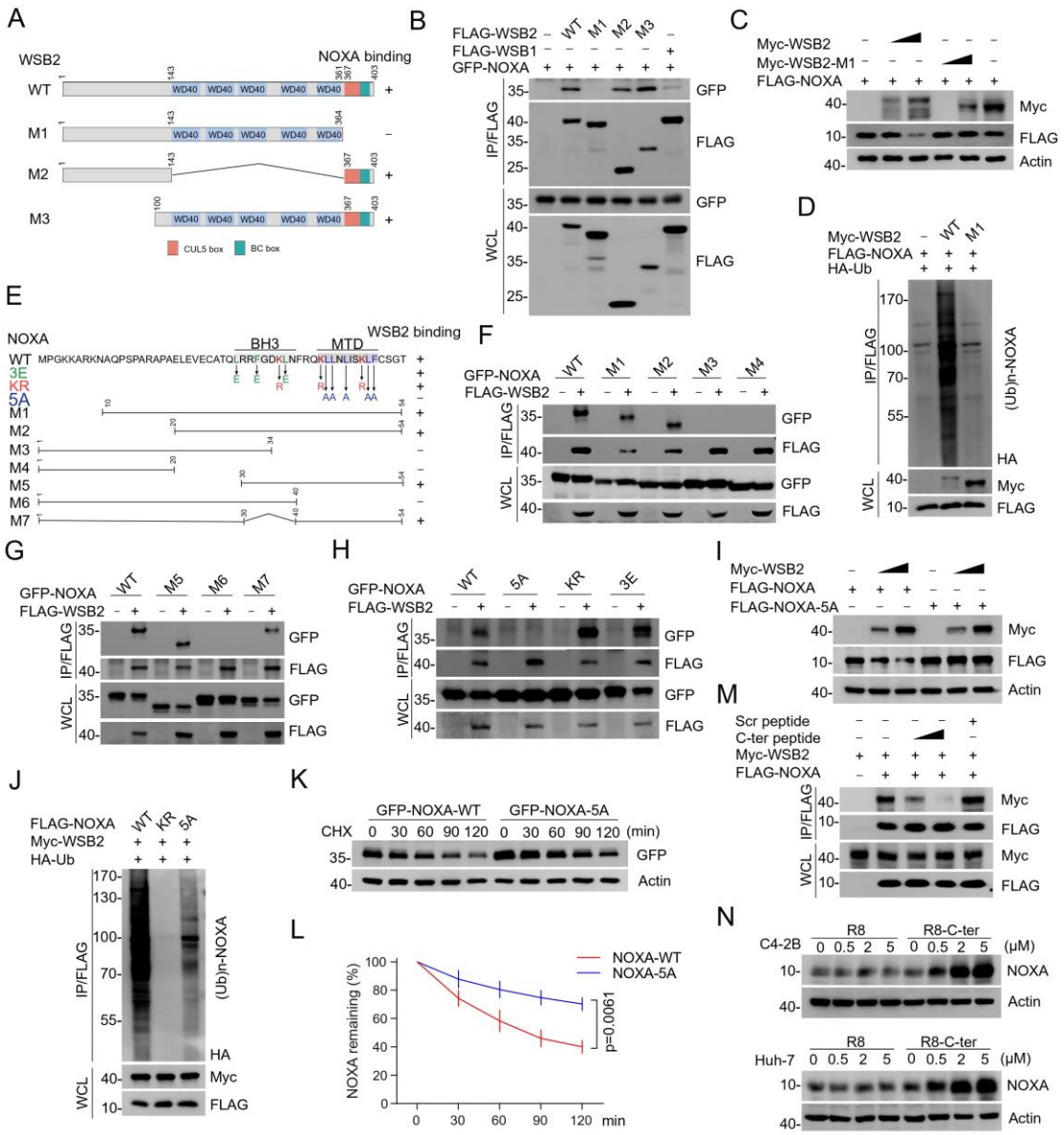

Figure 3. Identification of the mutual-binding regions of WSB2 and NOXA.

(**A**) Schematic representation of WSB2 deletion mutants.

(**B**) WB analyses of the indicated proteins in WCLs and co-IP samples of anti-FLAG antibody obtained from 293T cells transfected with the indicated plasmids.

(**C**) WB analyses of the indicated proteins in the WCL from 293 T cells transfected with the indicated plasmids.

(**D**) WB analyses of the products of *in vivo* ubiquitination assays performed using WCL from 293T cells transfected with the indicated plasmids for 24 h and treated with MG132(20 μM).

(**E**) Schematic representation of NOXA deletion or point mutants.

(**F-H**) WB analyses of the indicated proteins in the WCLs and co-IP samples of anti-FLAG

antibody obtained from 293T cells transfected with indicated plasmids.

(**I**) WB analyses of the indicated proteins in the WCL from 293 T cells transfected with the indicated plasmids.

(**J**) WB analyses of the products of *in vivo* ubiquitination assays performed using WCL from 293T cells transfected with the indicated plasmids and treated with MG132(20 μM).

(**K, L**) WB analyses of the indicated proteins in the WCL from 293 T cells transfected with the indicated plasmids treated with cycloheximide (CHX, 50 μg/ml) and harvested at different time points. (**L**) At each time point, the intensity of NOXA was normalized to the intensity of GAPDH and then to the value at 0 h. Data are shown as means ± SD (n=3). *P* values are calculated by the Two-way ANOVA test.

(**M**) 293T cells were transfected with the indicated plasmids. WSB2-NOXA complex was co-immunoprecipitated by anti-FLAG antibody, and then the bound complex was incubated with the increasing amounts of C-terminal NOXA peptide (200, 400 μg/ml) or the corresponding scramble peptide for 12 h. Bound material was subjected to WB analyses. C-ter: C-terminal NOXA peptide.

(**N**) WB analyses of the indicated proteins in WCLs from C4-2B and Huh-7 cells treated with the increasing concentration of C-terminal cell-penetrating peptide of NOXA or the corresponding R8 peptide for 12 h.

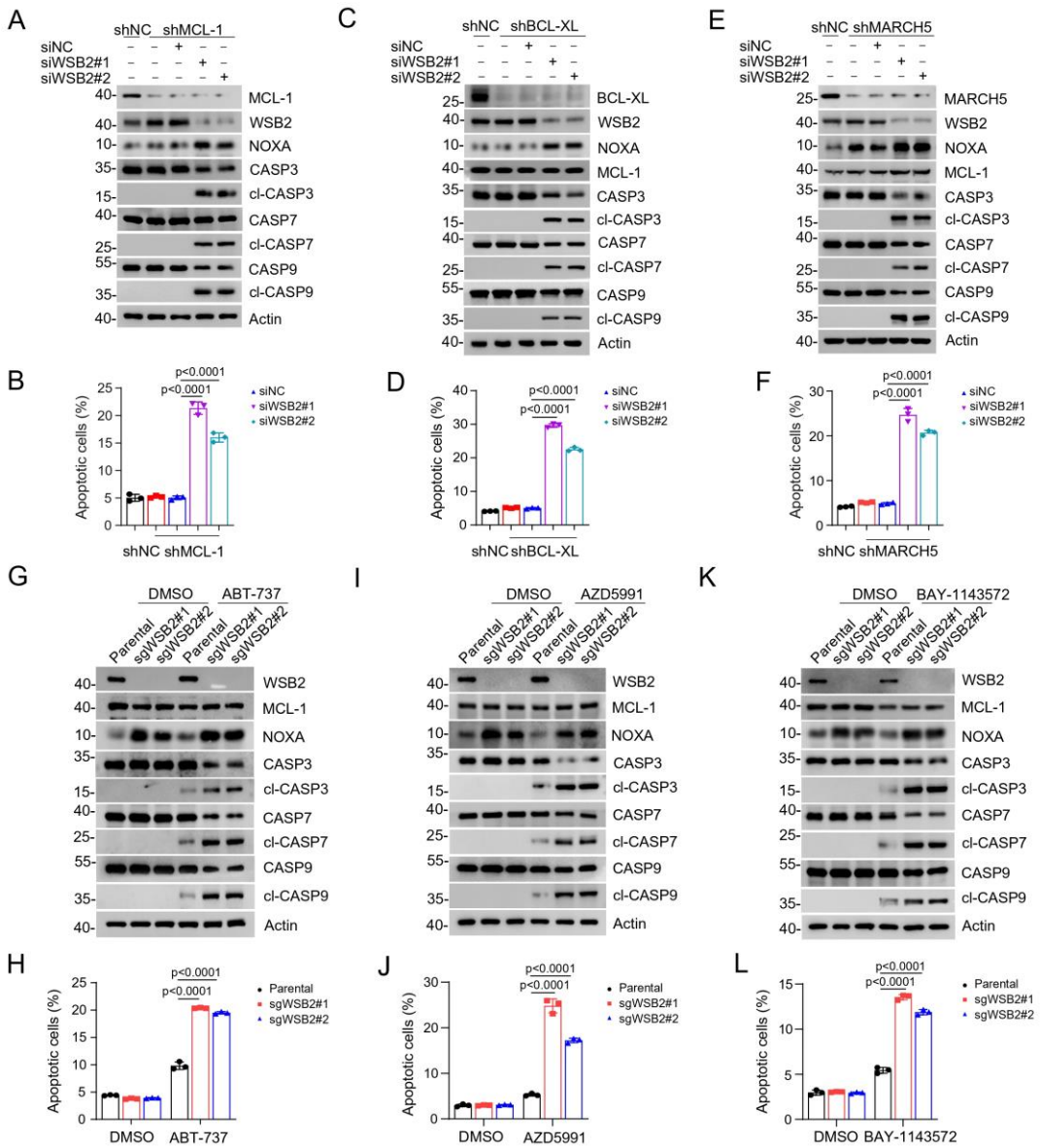

Figure 4. Combined inhibition of anti-apoptotic BCL-2 family members and WSB2 induces synthetic lethality.

(**A, B**) WB analyses of the indicated proteins in the WCL from C4-2B cells infected with lentivirus expressing BCL-XL-specific shRNA or NC and then transfected with the indicated siRNAs for 36 h. (**B**) Annexin-V-FITC/PI assays were used to stain the harvested cells in (A), of which later flow cytometry analysis was performed. Data are shown as means ± SD (n=3).

(**C, D**) Similar to (A, B), but MCL-1 was knocked down in C4-2B cells.

(**E, F**) Similar to (A, B), but MARCH5 was knocked down in C4-2B cells.

(**G, H**) WB analyses of the indicated proteins in the WCL from parental and WSB2 KO C4-2B cells treated with ABT-737 (20 μM) for 6 h. (**H**) Annexin-V-FITC/PI assays were used to stain

the harvested cells in (H), of which later flow cytometry analysis was performed. Data are shown as means ± SD (n = 3).

(**I, J**) Similar to (A, B), but AZD5991 (10 μM) was used for treatment in C4-2B cells.

(**K, L**) Similar to (A, B), but BAY-1143572 was used for treatment in C4-2B cells.

P values are calculated by the One-way ANOVA test in (B, D, F) and Two-way ANOVA test in (H, J, L), ns no significant.

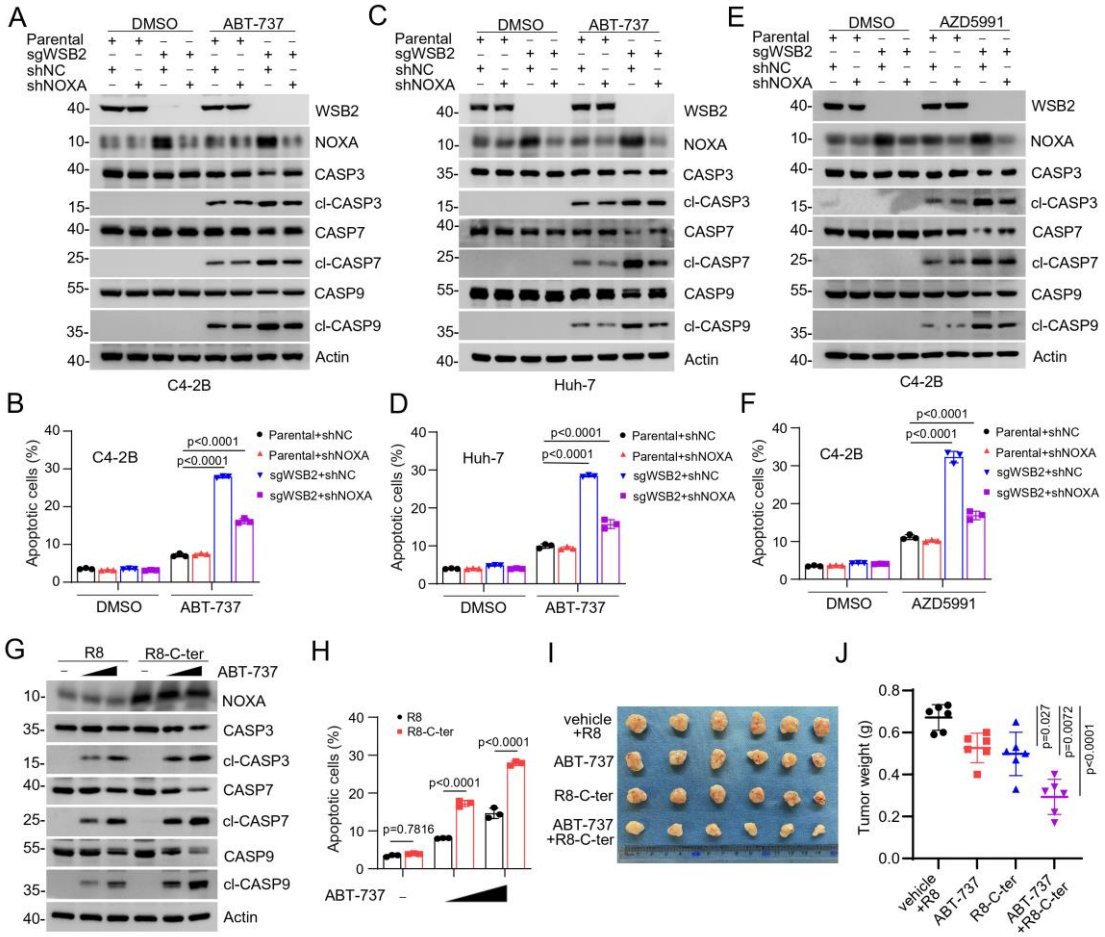

Figure 5. WSB2 primarily exerts its anti-apoptotic function largely via destabilizing NOXA.

(**A, B**) WB analyses of indicated proteins in WCLs from parental or WSB2 KO C4-2B cells infected with lentivirus expressing NOXA-specific shRNA or NC, treated with DMSO or ABT-737 (20 μM) for 6 h. (**B**) Annexin-V-FITC/PI assays were used to stain the harvested cells, of which later flow cytometry analysis was performed. Data are shown as means ± SD (n = 3).

(**C, D**) Similar to (A, B), but AZD5991 (10 μM) was used for treatment in C4-2B cells.

(**E, F**) Similar to (A, B), but Huh-7 cells were treated.

(**G, H**) WB analyses of the indicated proteins in the WCL from Huh-7 cells treated with the cell-penetrating C-terminal NOXA peptide (5 μM) or the corresponding scramble peptide (5 μM) for 12 h and then the cells were treated with increasing doses of ABT-737(10, 20 μM). Annexin-V-FITC/PI assays were used to stain the harvested cells, of which later flow cytometry analysis was performed. Data are shown as means ± SD (n = 3).

(**I, J**) Huh-7 cells were injected subcutaneously (s.c.) into the right flank of BALB/c mice and treated with ABT-737(30 mg/kg), R8-C-ter (20 mg/kg) or R8 (20 mg/kg) as control at different day points. 6 mice per experimental group. Tumors in each group at day 20 were harvested and photographed (I) and tumor weight (J) was documented. Data are shown as means ± SD (n = 6).

P values are calculated by the Two-way ANOVA test in (B, D, F, H).

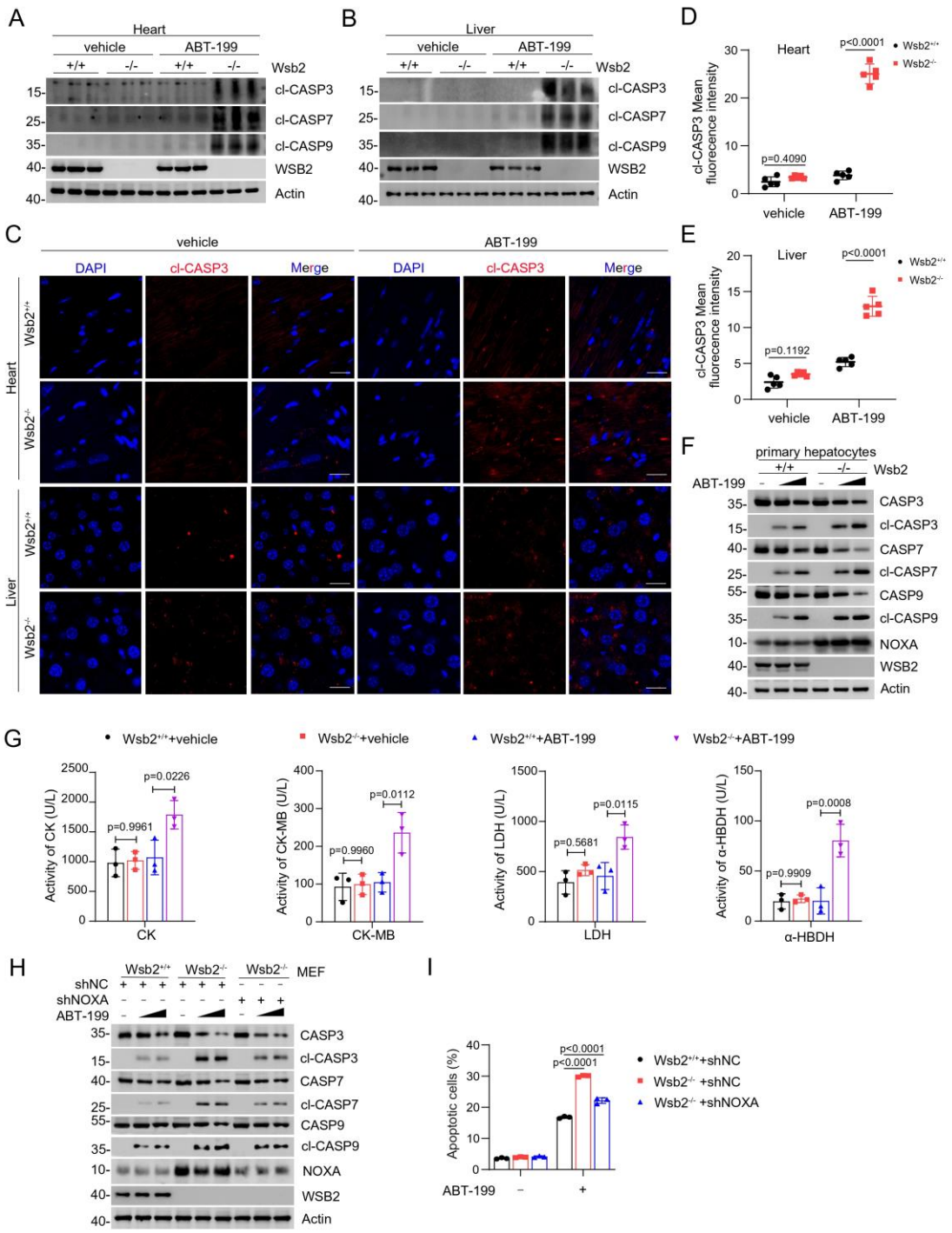

Figure 6. Validation of the anti-apoptotic function of WSB2 using Wsb2 KO mouse models.

(**A, B**) WB analyses of the indicated proteins in the WCL from heart (A) or liver (B) tissues obtained from Wsb2$^{+/+}$ and Wsb2$^{-/-}$ mice after gavage administration of vehicle or ABT-199 (100 mg/kg/day) for 7 days.

(**C**) Representative IF images from the heart or liver tissues of Wsb2$^{+/+}$ and Wsb2$^{-/-}$ mice after

oral administration of vehicle or ABT-199 (100 mg/kg/day) for 7 days, and stained with cl-CASP3 and DAPI. Scale bar, 20 μm.

(**D, E**) The mean fluorescence intensity of cl-CASP3 from the heart (D) or liver tissues (E) obtained from $Wsb2^{+/+}$ and $Wsb2^{-/-}$ mice. Data were shown as means ± SD (n = 5).

(**F**) WB analyses of the indicated proteins in the WCL from the primary hepatocytes of $Wsb2^{+/+}$ and $Wsb2^{-/-}$ mice treated with ABT-199 (10, 20 μM) for 6 h.

(**G**) The levels of myocardial zymogram in serum from $Wsb2^{+/+}$ and $Wsb2^{-/-}$ mice after gavage administration of vehicle or ABT-199 (100 mg/kg/day) for 7 days.

(**H, I**) WB analyses of indicated proteins in WCLs from $Wsb2^{+/+}$ and $Wsb2^{-/-}$ MEFs infected with lentivirus expressing NOXA-specific shRNA or NC, treated with DMSO or ABT-199 (20 μM) for 6 h. (**B**) Annexin-V-FITC/PI assays were used to stain the harvested cells, of which later flow cytometry analysis was performed. Data are shown as means ± SD (n = 3).

P values are calculated by the One-way ANOVA test in (G) and Two-way ANOVA test in (D, E).

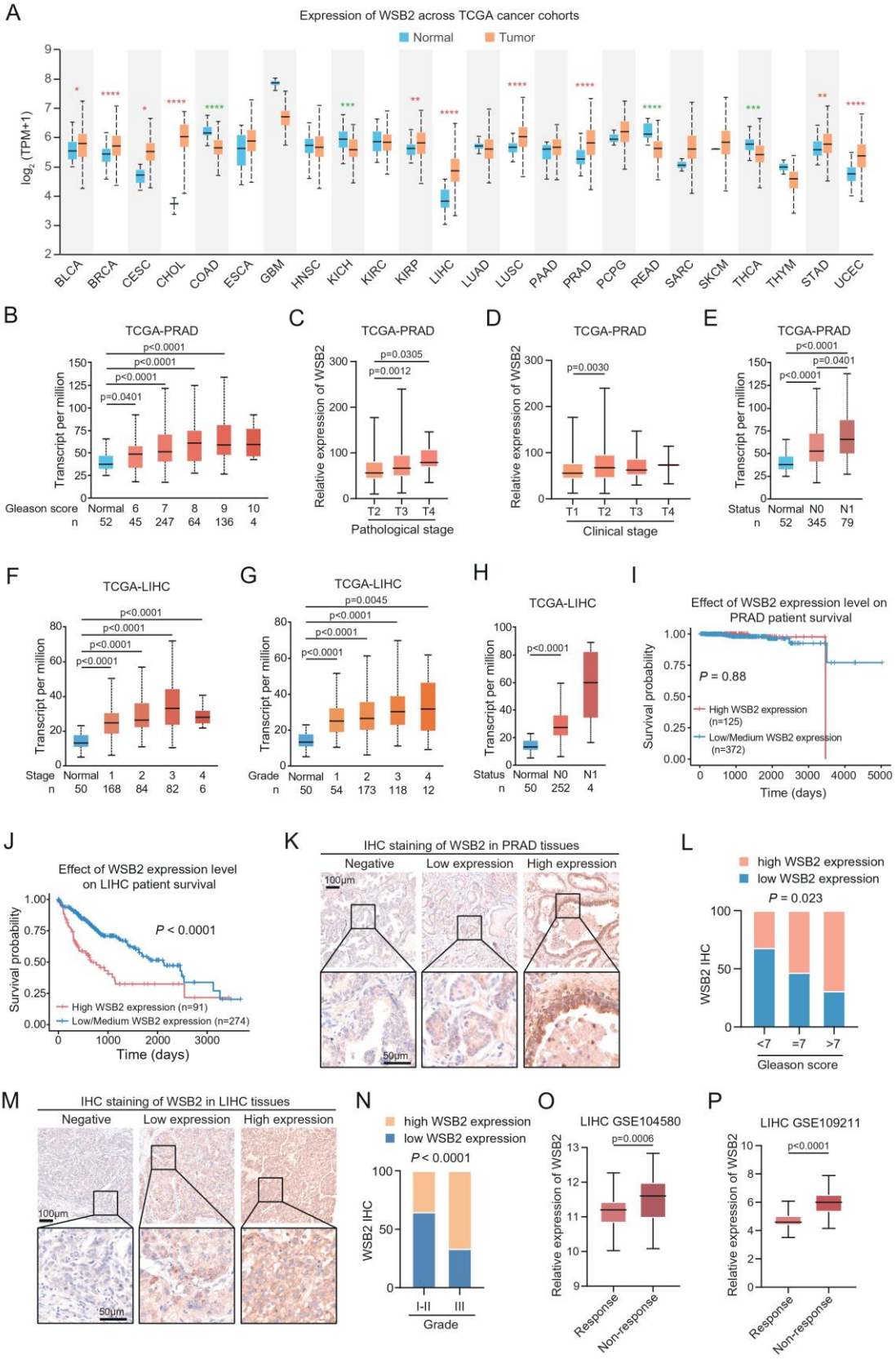

Figure 7. WSB2 expression is upregulated in multiple human cancers.

(**A**) WSB2 mRNA expression in normal and tumor tissues from the TCGA cohort.

(**B–E**) Relationship between WSB2 mRNA expression and Gleason score (B), nodal metastasis status (**C**), clinical T stage (**D**), and pathological T stage (E) in PRAD patients from the TCGA cohort.

(**F–H**) Relationship between WSB2 mRNA expression and clinical stage (**F**), pathological grade (**G**), and nodal metastasis status (**H**) in LIHC patients from the TCGA cohort.

(**I, J**) Kaplan–Meier survival plots of OS according to WSB2 mRNA expression in PRAD (**I**) and LIHC (**J**) patients from the TCGA cohorts.

(**K**) Representative IHC staining results for WSB2 in PRAD TMA, scale bar, 50 μm.

(**L**) Quantification analysis of WSB2 IHC staining in PRAD patients by Gleason score categories. n=84.

(**M**) Representative IHC staining results for WSB2 in LIHC TMA, scale bar, 50 μm.

(**N**) Quantification analysis of WSB2 IHC staining in LIHC patients by tumor grade categories. n=29.

(**O**) The WSB2 mRNA levels in 81 sorafenib-response and 66 sorafenib-non-response LIHC patients from GSE104580 dataset.

(**P**) The WSB2 mRNA levels in 42 sorafenib-response and 98 sorafenib-non-response LIHC patients from GSE109211 dataset.

P values are calculated by the unpaired *t* test in (A, B-H, L, N, O, P) and log-rank test in (I, J). *p < 0.05, **p < 0.01, ***p < 0.001, ****p < 0.0001.

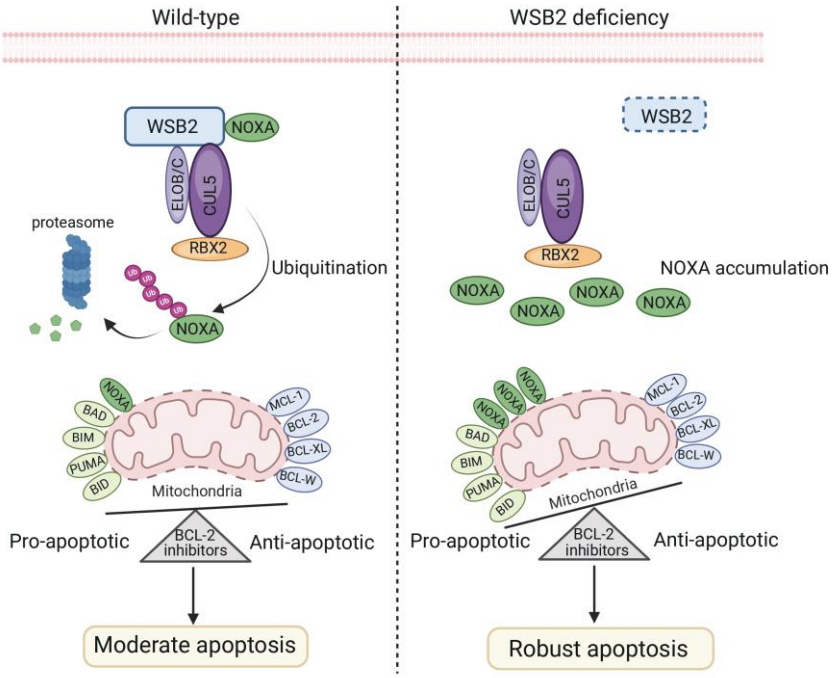

Figure 8. The schematic diagram illustrates that the disruption of the CRL5^{WSB2} E3 Ubiquitin ligase complex results in NOXA stabilization and increased sensitivity to BCL-2 family protein inhibitors.

Supplementary Materials for

Disruption of WSB2-mediated NOXA Degradation Induces Synthetic Lethality to Anti-apoptotic BCL-2 Family Protein Inhibitors

Figures. S1 to S5

Other Supplementary Materials for this manuscript include the following:

Table S1 to S6

Supplementary Table 1. Top 100 co-dependent genes of WSB2.

Supplementary Table 2. The GO analysis of top 500 co-dependent genes of WSB2.

Supplementary Table 3. The DepLink analysis of top correlated drugs with WSB2.

Supplementary Table 4. Sequence information.

Supplementary Table 5. Antibody information.

Supplementary Table 6 Cell cultures, chemicals, and Kits.

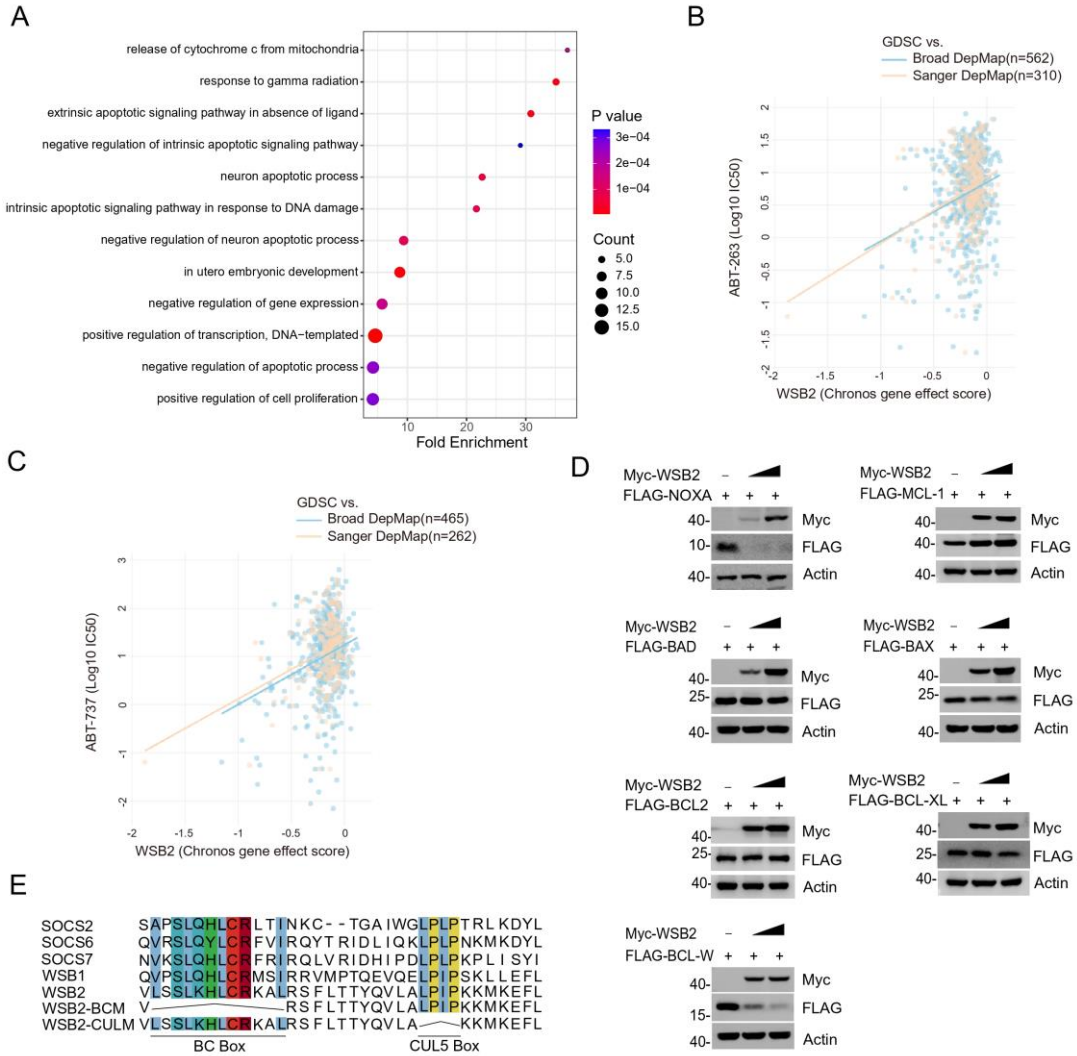

Supplementary Figure 1. WSB2 interacts with NOXA and promotes its degradation (related to Figure. 1, 2).

(A) GO enrichment analysis of biological processes was performed on the top 100 co-dependent genes of WSB2 in the Broad's 21Q2 DepMap dataset. The biological processes were ranked based on fold enrichment values, with the most significant processes highlighted in red and the less significant processes highlighted in blue, according to log10(FDR) values. In the graph, larger dots represent a higher number of genes involved in a particular process. **(B)** Gene effect scores of query gene and the drug selected from Panel 1H. Each dot is a cell line of the selected cancer type(s). Drug sensitivity is represented by log-fold change (PRISM) or IC50 (GDSC), where a more negative value denotes stronger treatment response. **(C)** WB analyses of the indicated proteins in WCLs from 293 T cells transfected with the

indicated plasmids.

(D) The canonical BC box and CUL5 box sequences of WSB2, as well as the amino acid deletions corresponding to each mutant, are indicated.

(E) WB analyses of the indicated proteins in the WCLs from 293 T cells transfected with the indicated plasmids.

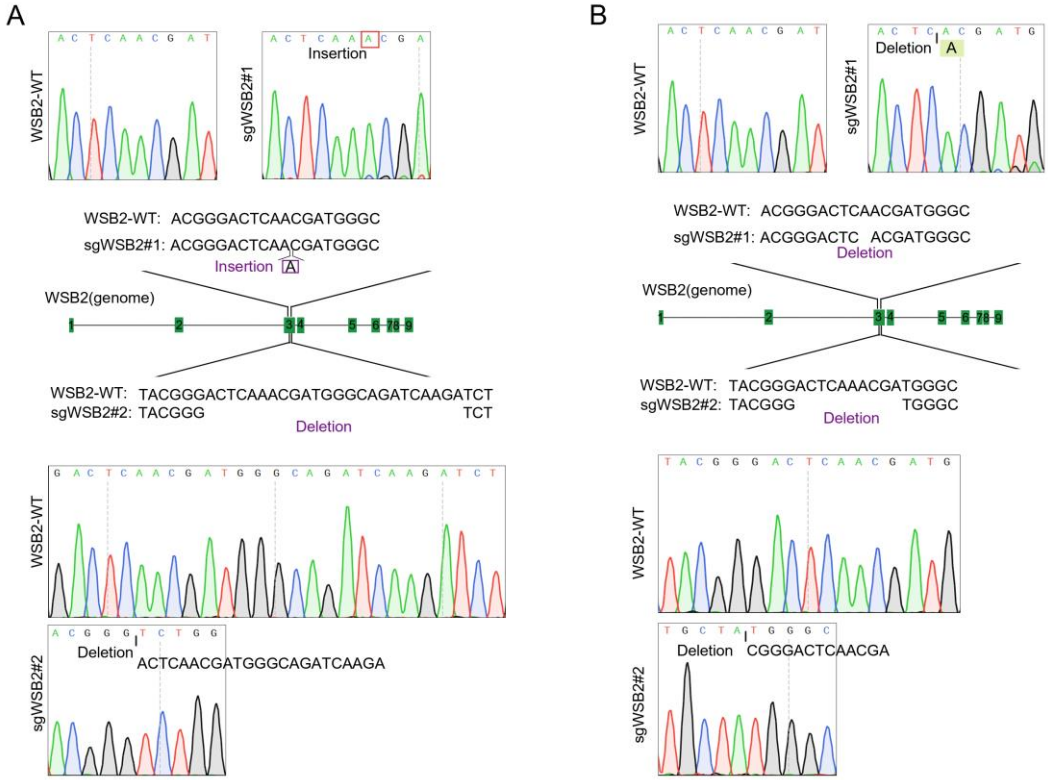

Supplementary Figure 2. Validation of WSB2 knockout in two cancer cell lines.

(A) Schematic of CRISPR/Cas9-mediated knockout of WSB2 by sgRNA#1 or sgRNA#2 in C4-2B cells. Sanger sequencing confirming that the *WSB2* gene was edited by sgRNA#1 or sgRNA#2 in C4-2B cells.

(B) Schematic of CRISPR/Cas9-mediated knockout of WSB2 by sgRNA#1 or sgRNA#2 in Huh-7 cells. Sanger sequencing confirming that the *WSB2* gene was edited by sgRNA#1 or sgRNA#2 in Huh-7 cells.

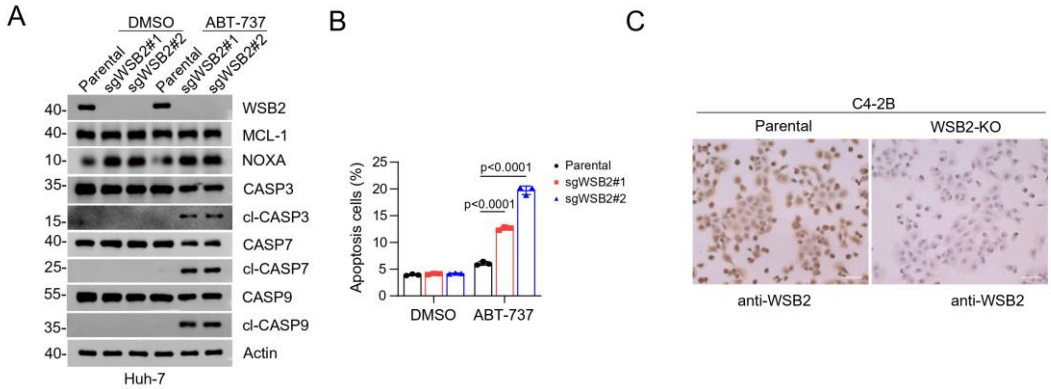

Supplementary Figure 3. The combination of WSB2 KO and ABT-737 treatment induces robust apoptosis in Huh-7 cells (related to Figure 7).

(A) WB analyses of the indicated proteins in WCLs from parental and WSB2 KO Huh-7 cells treated with DMSO or ABT-737 (20 μM) for 6 h.

(B) Annexin-V-FITC/PI assays were used to stain the harvested cells in (A), of which later flow cytometry analysis was performed. Data are shown as means ± SD (n = 3). *P* values are calculated by the Two-way ANOVA test.

(C) IHC analysis of parental and WSB2 KO C4-2B cells from cultures on glass slides using an anti-DPP9 antibody. Representative staining results are shown. Scale bars, 100 μm.

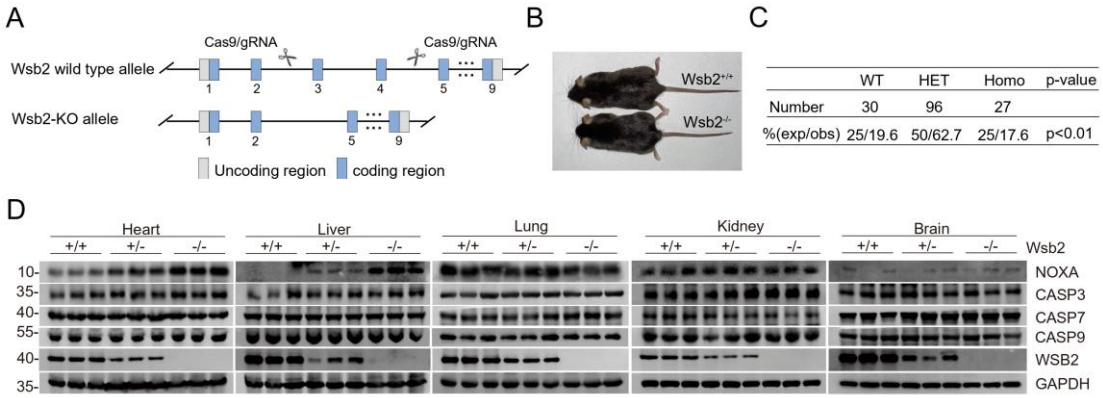

Supplementary Figure 4. Generation and Validation of Wsb2 KO mouse models (related to Figure 6).

(A) Strategy to generate Wsb2 KO mice using CRISPR/Cas9 methods.

(B) Representative images of male Wsb2$^{-/-}$ and matched Wsb2$^{+/+}$ mice at 3 months of age.

(C) Genotyping analysis of offspring from mating between Wsb2 heterozygous mice at P10. *P* values are calculated by the Chi-Squared Test.

(D) WB analyses of the indicated proteins in WCL from the indicated tissues of Wsb2$^{+/+}$ and Wsb2$^{-/-}$ mice.

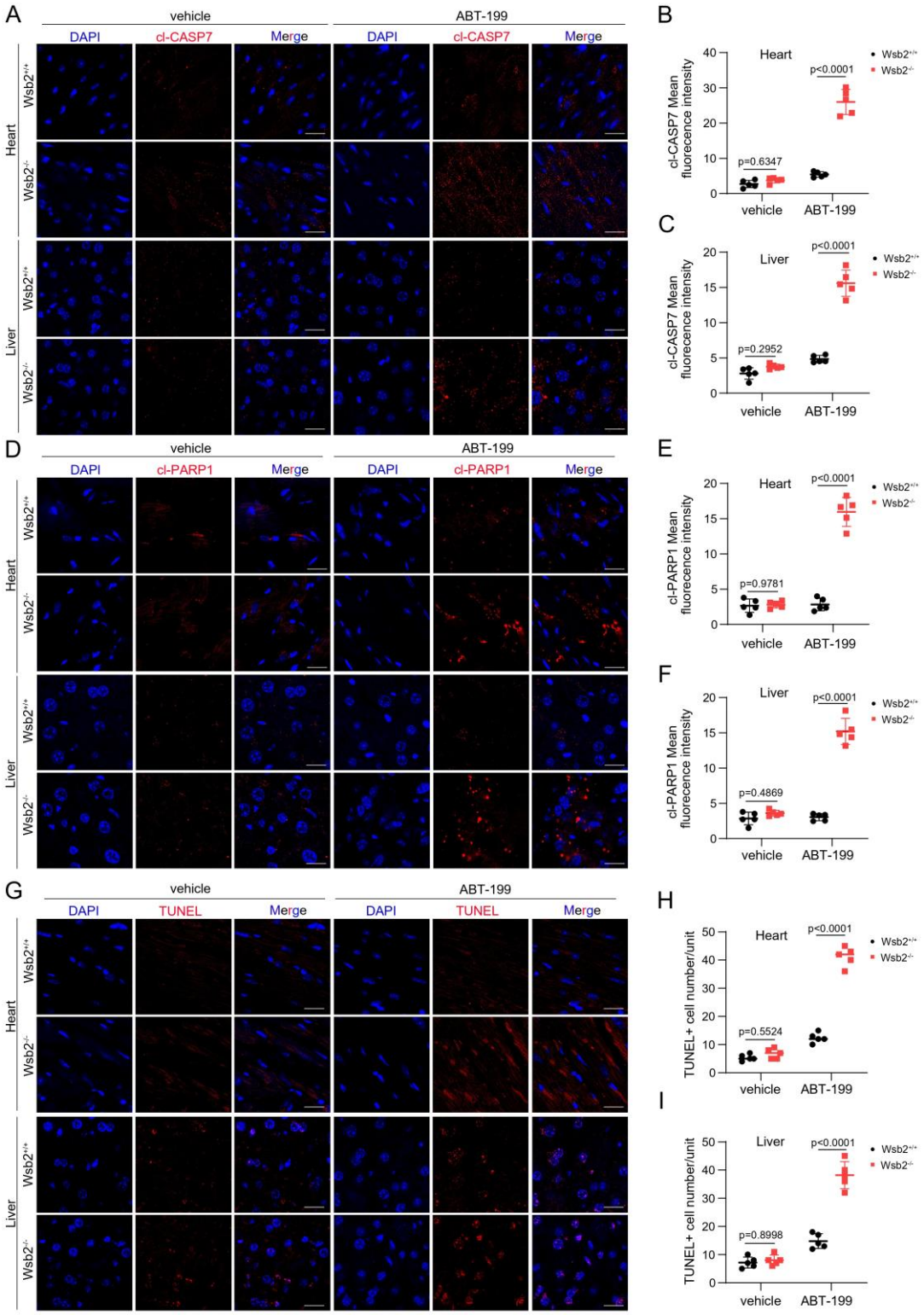

Supplementary Figure 5. The deficiency of WSB2 enhances the susceptibility of ABT199-induced apoptosis in the heart and liver tissues of Wsb2 KO mice (related to Figure 6).

(**A**) Representative IF images from the heart or liver tissues of Wsb2$^{+/+}$ and Wsb2$^{-/-}$ mice after

oral administration of vehicle or ABT-199 (100 mg/kg/day) for 7 days, and stained with cl-CASP7 and DAPI. Scale bar, 20 μm.

(**B, C**) The mean fluorescence intensity of cl-CASP7 from the heart (B) or liver tissues (C) obtained from $Wsb2^{+/+}$ and $Wsb2^{-/-}$ mice. Data were shown as means ± SD (n = 5).

(**D**) Representative IF images from the heart or liver tissues of $Wsb2^{+/+}$ and $Wsb2^{-/-}$ mice after oral administration of vehicle or ABT-199 (100 mg/kg/day) for 7 days, and stained with cl-PARP1 and DAPI. Scale bar, 20 μm.

(**E, F**) The mean fluorescence intensity of cl-PARP1 from the heart (E) or liver tissues (F) obtained from $Wsb2^{+/+}$ and $Wsb2^{-/-}$ mice. Data were shown as means ± SD (n = 5).

(**G**) Representative IF images from the heart or liver tissues of $Wsb2^{+/+}$ and $Wsb2^{-/-}$ mice after oral administration of vehicle or ABT-199 (100 mg/kg/day) for 7 days, and stained with TUNEL and DAPI. Scale bar, 20 μm.

(H, I) The $TUNEL^{+}$ cell number in the heart (H) or liver tissues (I) obtained from $Wsb2^{+/+}$ and $Wsb2^{-/-}$ mice. Data were shown as means ± SD (n = 5). Data were shown as means ± SD (n = 5).

P values are calculated by the Two-way ANOVA test in (B, C, E, F, H, I).